Dynamic evolution of damage by microcracking with heat dissipation

Cristian Dascalu, Kokouvi Gbetchi

Dynamic evolution of damage by microcracking with heat dissipation

Cristian Dascalu, Kokouvi Gbetchi

Université de Lorraine, CNRS, Arts et Métiers ParisTech, LEM3, F-57000 Metz, France

---

Abstract

A new thermo-mechanical damage model is constructed in the present contribution using a two-scale approach. The model is deduced from microstructures with microcracks evolving dynamically in a nominally brittle material and for which the fracture energy dissipated at the moving tips is converted to heat. The use of an homogenization method based on asymptotic developments leads to a damage evolution law coupled with the macroscopic thermoelasticity system. The obtained model accounts for inertial effects, thermo-elastic coupling and heat dissipation effects due to damage propagation. The local effective response of the model is analyzed with special emphasis on thermal evolutions. Strain-rate and microstructural size effects are illustrated. Cooling and heating regimes associated to damage initiation and propagation are identified and analyzed for different values of the model parameters. Results of numerical simulations for a compact compression test are presented and compared with the experimental data for temperature field measurements during rapid failure of PMMA samples. Good agreement is found between the model predictions and the measured thermal evolution.

Keywords: Micro-cracks, dynamic propagation, crack-tip heating, homogenization, damage law, thermal dissipation, impact test, PMMA

4 septembre 2019

1. Introduction

The evolution of microcracks plays an essential role in the rapid failure of brittle materials like ceramics, rocks or polymers. This was clearly proved, for instance, by the experimental observations of Ravi-Chandar and Knauss (1984); Sharon et al. (1996); Ravi-Chandar and Yang (1997); Sharon et al. (1999); Dalmas et al. (2013) on the dynamic fracture of nominally brittle polymers. The morphology of the fracture surface reveals that nucleation, growth and coalescence of microcracks represent the dominant failure micromechanism. The formation of microbranches on the main crack faces can explain the dramatic increase of dissipated energy and the saturation effects in the crack-tip velocity below the theoretical limit speed.

Despite the important progresses of Fracture Mechanics to reproduce the dynamic effects of failure (e.g., Freund, 1990; Ravi-Chandar, 2004), the theory has limited predictive capacity for complex rupture patterns. The case of microbranching instabilities is an example among others. The reported microscopic observations during fast failure in brittle materials suggest that a proper model could be obtained by incorporating the microcracking mechanism. Since it takes place at scales smaller than that of the solid structure, a multiscale appproach with propagating microcracks may represent the appropriate modeling framework.

The thermo-mechanical couplings represent another significant aspect of the fast failure in brittle solids. Temperature measurements for opening mode cracks, like those reported in Fuller et al. (1975); Weichert and Schönert (1978); Rittel (1998, 1999); Bougaut and Rittel (2001); Bjerke and Lambros

(2003) for glass and PMMA materials, revealed a significant temperature rise in a highly localized area surrounding the crack tip during propagation and a temperature drop ahead the crack-tip in the fracture initiation phase. After a cooling regime prior to crack initiation, during the rapid mode I growth the crack tip behaves like a moving heat source. Since the plasticity effects can be neglected and the energy needed for the new crack surface formation is much smaller that the total energy expended in the crack tip region, other dissipative processes, like the craze formation and breakdown in polymers (as discussed in Bjerke and Lambros, 2003; Estevez et al., 2005), are responsible for the tip heating effect.

In order to describe these specific thermal behaviors it is necessary to adequately model the thermo-mechanical coupling at the front of a running crack. In particular, one needs to establish the link between the energy dissipation at the moving tip and the corresponding heat generation. Attempts to model such thermofracture heating effects in the context of Fracture Mechanics have been made for instance in Bui et al. (1980, 1986); Sun and Hsu (1996). These authors consider crack models with Dirac-type heat sources located at the tip point and which intensity represents the excess of energy release rate with respect to that necessary for the new crack surface formation.

More recently, Bjerke and Lambros (2003) proposed a thermally dissipative cohesive zone model for dynamic fracture of amorphous polymers. Their model is based on the assumption that the excess supplied energy in the crack-tip region is converted to heat within the cohesive zone that models the crazing process. A model involving heat generation by plastic dissipation

in the bulk and a thermal cohesive-zone has been studied in Estevez et al. (2005) under quasi-static conditions. As concerns the dynamic failure approach of Bjerke and Lambros (2003), comparison with experiments showed good agreement for the low speed fracture case, i.e. crack-tip speed up to $0.2C_R$, where C_R is the Rayleigh wave velocity. For faster cracks, the authors comment : "For higher speed fracture where subsurface damage becomes prominent, the line dissipation model of a cohesive zone is inadequate, and a distributed damage model is needed". To our knowledge, a damage model able to predict the heating effects during rapid failure in brittle materials has not been proposed in the literature and this is the aim of the present contribution.

The distributed damage approaches proved to be an efficient tool to model dynamic failure in brittle materials. Phenomenological rate-dependent models have been considered by introducing viscous-type damage laws (e.g. Dubé et al., 1996; Allix et al., 2003; Suffis et al., 2003) or gradient damage and phase-field models (e.g. Bourdin et al., 2011; Spatschek et al., 2011; Borden et al., 2016; Hofacker et al., 2012; Schlüter et al., 2014; Li et al., 2016). Extensions that incorporate the thermo-mechanical couplings are given in Miehe et al. (2015); Schlüter et al. (2014); Chu et al. (2017). Microcrack informed models were proposed in the dynamic failure context, among other contributions, in Nemat-Nasser and Deng (1994); Ravichandran and Subhash (1995); Huang et al. (2002); Paliwal and Ramesh (2008); Bhatt et al. (2012); Keita et al. (2014); Hu et al. (2015).

The objective of the present work is to construct a two-scale thermomecanical damage model in dynamics that accounts for microcracks evolution

and thermofracture heating effect. Although the rapid failure processes can be reasonably described under adiabatic conditions at the macroscopic scale, the microscopic conduction effects may still be important. This motivates the adoption of the point heat source model (Bui et al., 1980, 1986; Sun and Hsu, 1996) at the small-scale level, at the moving tips of the microcracks. The propagation of microcracks is assumed to follow a Griffith type criterion formulated with the dynamic energy release rate.

Starting with the fully coupled dynamic thermoelastic fracture problem at the microscale, we use the homogenization method developed in Dascalu et al. (2008); Keita et al. (2014); Dascalu (2018), based on asymptotic developments, to obtain the new thermo-damage model. The upscaling procedure leads to distributed heat sources, depending on the damage energy-release rate, in the homogenized temperature equation and a damage evolution law expressed with the thermal and the mechanical fields.

Investigations of the local response of the new model are performed to illustrate its capacity for predicting strain-rate and microstructural size effects and specific thermal behaviors like the existence of cooling and heating regimes associated, respectively, to damage initiation and propagation. Structural numerical simulations are also performed to reproduce the temperature field measurements during rapid failure of PMMA samples in a Compact Compression Test (Rittel, 1998, 1999; Bougaut and Rittel, 2001), showing good agreement between theoretical predictions and experimental results.

The paper is organized as follows. In Section 2 we formulate the thermoelastic fracture problem for a solid with a distribution of microcracks propagating dynamically. The asymptotic homogenization analysis is performed in

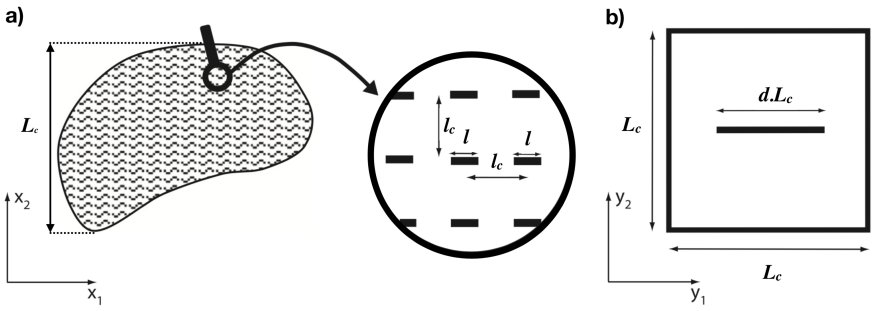

FIGURE 1: a) Micro-fissured medium with locally periodic microstructure with l_c the size of a period, l the local micro-crack length and L_c the characteristic length of the macro-structure. b) Reference cell of size L_c with rescaled crack length $d.L_c$.

Section 3 for the thermoelasticity system and in Section 4 for the damage evolution law. Numerical simulations of the local effective response of the model are presented in Section 5. The results of structural computations for the Compact Compression Test in PMMA samples and the comparison with the experimental data are given in the last section.

2. Two-scale thermoelastic fracture problem

Consider a solid containing a large number of small cracks. When their lengths are much smaller than the size of the whole structure, we distinguish between the macroscopic properties at the scale of the solid body and the microscopic ones characterizing the local behavior in the vicinity of one microcrack.

The distribution of microcracks in the solid is assumed to be locally periodic, as illustrated in Figure 1, all of them being straight and parallel to the x_1 axis.

Let l be the microcrack length and l_c the size of the periodicity cells. The local periodicity means slow small-scale variations of l, with fixed l_c, such that locally the microstructure may be considered periodic.

If L_c is a characteristic length of the macrostructure, as illustrated in Figure 1, we introduce the parameter

$$\varepsilon = \frac{l_c}{L_c} \tag{1}$$

as a mesure of the difference between microscopic and macroscopic scales of the solid body.

We consider plane strain deformations and we denote by $\mathcal{B}$ the two-dimensional solid domain and by $\mathcal{C}$ the union of all the micro-cracks inside $\mathcal{B}$. The coupled nonlinear equations of dynamic thermoelasticity :

$$c\frac{\partial T^\varepsilon}{\partial t} + \alpha(3\lambda + 2\mu)T^\varepsilon \frac{\partial e_{xjj}(\mathbf{u}^\varepsilon)}{\partial t} + \frac{\partial q_j^\varepsilon}{\partial x_j} = 0 \tag{2}$$

$$\rho\frac{\partial^2 u_i^\varepsilon}{\partial t^2} - \frac{\partial \sigma_{ij}^\varepsilon}{\partial x_j} = 0 \tag{3}$$

hold true in the solid part of $\mathcal{B}$. Here c is the specific heat, α is the coefficient of thermal expansion, λ and μ are the Lamé elastic coefficients and ρ is the mass density.

The relation (2) is the nonlinear form of the temperature equation. Since thermoelastic fracture problems may involve important temperature variations, in our analysis we will follow Bui et al. (1980, 1986) by using the non-linearized thermal equation.

The temperature field T^ε and the heat flux $\boldsymbol{q}^\varepsilon$ are related by Fourier law :

$$q_j^\varepsilon = -k\frac{\partial T^\varepsilon}{\partial x_j} \tag{4}$$

with k the heat conduction coefficient.

The components of the strain tensor calculated with respect to x_i variables using the displacement field $\mathbf{u}^\varepsilon$ are denoted by $e_{xkl}(\mathbf{u}^\varepsilon) = \frac{1}{2}\left(\frac{\partial u_k^\varepsilon}{\partial x_l} + \frac{\partial u_l^\varepsilon}{\partial x_k}\right)$ and the constitutive law for the stress tensor $\boldsymbol{\sigma}^\varepsilon$ in an isotropic solid reads :

$$\sigma_{ij}^\varepsilon = \lambda e_{xkk}(\mathbf{u}^\varepsilon)\delta_{ij} + 2\mu e_{xij}(\mathbf{u}^\varepsilon) - \alpha(3\lambda + 2\mu)(T^\varepsilon - T_0)\delta_{ij} \tag{5}$$

with T_0 being the initial temperature.

Traction-free and thermally isolating boundary conditions are assumed on the crack faces

$$\boldsymbol{\sigma}^\varepsilon \mathbf{N} = 0 \qquad ; \qquad \boldsymbol{q}^\varepsilon \mathbf{N} = 0 \tag{6}$$

where $\mathbf{N}$ is the unit normal vector on the crack line, as shown in Fig. 2. Additional conditions on the outer boundary of $\mathcal{B}$ and initial conditions for the temperature, displacement and velocity fields inside the solid domain should be specified for the formulation of the thermoelastic problem.

The dynamic propagation of microcracks is described by a Griffith criterion involving the energy-release rate (Freund, 1990; Ravi-Chandar, 2004) :

$$\mathcal{G}^{d\varepsilon} = \lim_{r\to 0} \int_{\Gamma_r} ((\mathcal{U}^\varepsilon + \mathcal{K}^\varepsilon)n_1 - \sigma_{ij}^\varepsilon n_j \frac{\partial u_i^\varepsilon}{\partial x_1})ds \tag{7}$$

expressing the available energy for crack propagation. Here Γ_r is a closed circular contour of radius r encircling the crack tip and $\mathbf{n}$ is its outward unit normal, as represented in Figure 2. $\mathcal{U}^\varepsilon$ is the internal energy :

$$\mathcal{U}^\varepsilon = \frac{1}{2}(\lambda e_{xii}(\mathbf{u}^\varepsilon)e_{xjj}(\mathbf{u}^\varepsilon) + 2\mu e_{xij}(\mathbf{u}^\varepsilon)e_{xij}(\mathbf{u}^\varepsilon)) + (3\lambda + 2\mu)\alpha T_0 e_{xkk}(\mathbf{u}^\varepsilon) + cT^\varepsilon \tag{8}$$

and $\mathcal{K}^\varepsilon$ is the kinetic energy :

$$\mathcal{K}^\varepsilon = \frac{1}{2}\rho \frac{\partial \mathbf{u}^\varepsilon}{\partial t}\frac{\partial \mathbf{u}^\varepsilon}{\partial t} \tag{9}$$

Microcracks propagate when $\mathcal{G}^{d\varepsilon} = \mathcal{G}_c$, with $\mathcal{G}_c$ being the critical fracture energy of the material.

The heat flow from a crack tip during propagation can be defined as the limit

$$D^{\varepsilon} = \lim_{r \to 0} \int_{\Gamma_r} \boldsymbol{q}^{\varepsilon} \mathbf{n} \, ds \tag{10}$$

Following the approaches of Bui et al. (1980, 1986), Sun and Hsu (1996), we consider the crack tips as moving heat sources. A part 2γ of the energy dissipated during fracture is needed for the formation of new crack surfaces while the rest is converted to heat through specific material failure mechanisms, like the process of craze formation and breakdown in brittle amorphous polymers. If we denote by $v_p = \frac{1}{2}\frac{dl}{dt}$ the velocity of a microcrack tip, then the local energy balance during its propagation reads

$$D^{\varepsilon} = v_p(\mathcal{G}^{d\varepsilon} - 2\gamma) \tag{11}$$

For some materials the surface energy term 2γ is negligible when compared with the energy release rate $\mathcal{G}^{d\varepsilon}$. As Bjerke and Lambros (2003) remark, the surface energy of some polymers is several orders of magnitude lower than the fracture energy. For example, Berry (1960) estimates the surface energy of PMMA as 0.1 J/m^2 while the measured values of the energy release rate are 3-4 orders of magnitude higher, depending on the crack velocity. In the case of polystyrene, Wool (1995) reported a surface energy of 0.04 J/m^2, which is negligible in comparison to the critical fracture energy.

In this case, (11) can be replaced by the approximate relation

$$D^{\varepsilon} = v_p \mathcal{G}^{d\varepsilon} \tag{12}$$

In what follows, the relation (12) will be adopted. However, the present approach may be easily adapted to the case of non-negligible surface energy, by replacing the equation (12) by (11).

The relations (10-12) express the link between the energy dissipation and the heat production during failure and represent a supplementary condition to be imposed at the moving tips of microcracks. This condition introduces a new thermo-mechanical coupling for the solid body.

3. Asymptotic developments and homogenization analysis

The asymptotic homogenization method (Sanchez-Palencia, 1980; Fish, 2013) is employed in this section to obtain the macroscopic thermoelasticity equations from the initial problem described previously. For bodies without cracks, similar techniques have been used in coupled dynamic thermoelasticity by Ene (1983); Francfort (1983); Parnell (2006); Auriault (2012) among other authors. In the present development we focus on the influence of microcracks with the specific singularities of the fields, the damage dependence of the effective thermoelastic coefficients and the upscaling of the temperature equation with the non-classical heat source conditions.

In the previous section, the characteristic length of the microstructure l_c has been introduced as the size of the microscopic period and also the mutual distance between neighbor microcracks. The damage variable d may be defined as the normalized microcrack length :

$$d = \frac{l}{l_c} \tag{13}$$

The local periodicity assumption for the length l allows for large-scale spatial variations of the damage variable d.

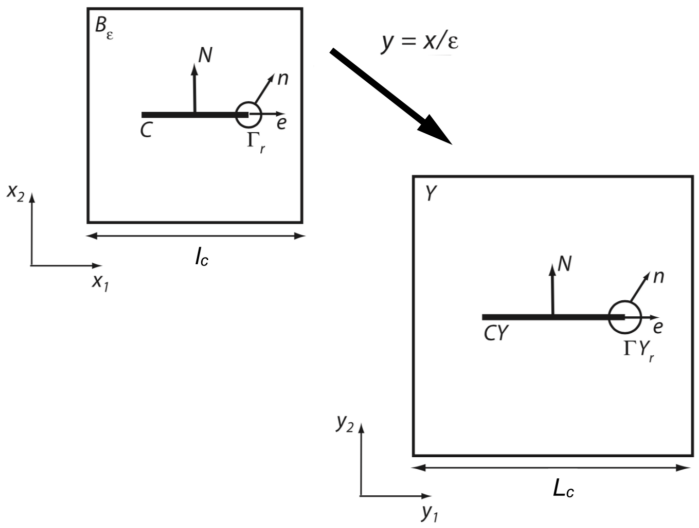

FIGURE 2: Scaling of the microscopic period of the material to the reference cell.

To characterize the field variations at different scales, we distinguish between the macroscopic variable $\mathbf{x}$ and the microscopic variable $\mathbf{y}$, linked by the relation $\mathbf{y} = \frac{\mathbf{x}}{\varepsilon}$, with ε defined in (1). The scaling of the microscopic period by this transformation leads to a reference cell Y, of size L_c and containing the crack CY of length $d.L_c$, as illustrated in Figure 2.

For a field f depending on both $\mathbf{x}$ and $\mathbf{y}$, the total spatial derivative can be calculated by the formula $\frac{df}{dx_i} = \frac{\partial f}{\partial x_i} + \frac{1}{\varepsilon}\frac{\partial f}{\partial y_i}$.

In what follows, we adopt the separation of scales assumption

$$\varepsilon = \frac{l_c}{L_c} \ll 1 \tag{14}$$

This means that the scale of microcracks is small in comparison with that of the solid body. Variations in $\mathbf{y}$ do not have much influence on $\mathbf{x}$ and both variables should be taken into account in the description of the physical fields, being treated as independent variables.

The displacement $\mathbf{u}^\varepsilon$ and the temperature T^ε fields are developed with respect the the small parameter ε in the form :

$$\mathbf{u}^\varepsilon(\mathbf{x},t) = \mathbf{u}^{(0)}(\mathbf{x},\mathbf{y},t) + \varepsilon\mathbf{u}^{(1)}(\mathbf{x},\mathbf{y},t) + \varepsilon^2\mathbf{u}^{(2)}(\mathbf{x},\mathbf{y},t) + ... \tag{15}$$

$$T^\varepsilon(\mathbf{x},t) = T^{(0)}(\mathbf{x},\mathbf{y},t) + \varepsilon T^{(1)}(\mathbf{x},\mathbf{y},t) + \varepsilon^2 T^{(2)}(\mathbf{x},\mathbf{y},t) + ... \tag{16}$$

where $\mathbf{u}^{(i)}(\mathbf{x},\mathbf{y},t)$ and $T^{(i)}(\mathbf{x},\mathbf{y},t)$, $\mathbf{x} \in B$, $\mathbf{y} \in Y$ are Y-periodic.
Using these developments in the equations (4-5) we obtain :

$$\boldsymbol{\sigma}^\varepsilon(\mathbf{x},t) = \frac{1}{\varepsilon}\boldsymbol{\sigma}^{(-1)}(\mathbf{x},\mathbf{y},t) + \boldsymbol{\sigma}^{(0)}(\mathbf{x},\mathbf{y},t) + \varepsilon\boldsymbol{\sigma}^{(1)}(\mathbf{x},\mathbf{y},t) + \varepsilon^2\boldsymbol{\sigma}^{(2)}(\mathbf{x},\mathbf{y},t) + ... \tag{17}$$

$$\boldsymbol{q}^\varepsilon(\mathbf{x},t) = \frac{1}{\varepsilon}\boldsymbol{q}^{(-1)}(\mathbf{x},\mathbf{y},t) + \boldsymbol{q}^{(0)}(\mathbf{x},\mathbf{y},t) + \varepsilon\boldsymbol{q}^{(1)}(\mathbf{x},\mathbf{y},t) + \varepsilon^2\boldsymbol{q}^{(2)}(\mathbf{x},\mathbf{y},t) + ... \tag{18}$$

where

$$\sigma_{ij}^{(-1)} = \lambda e_{ykk}(\mathbf{u}^{(0)})\delta_{ij} + 2\mu e_{yij}(\mathbf{u}^{(0)}) \tag{19}$$

$$\begin{aligned}\sigma_{ij}^{(0)} = {} & \lambda(e_{xkk}(\mathbf{u}^{(0)}) + e_{ykk}(\mathbf{u}^{(1)}))\delta_{ij} + 2\mu(e_{xij}(\mathbf{u}^{(0)}) + e_{yij}(\mathbf{u}^{(1)})) \\ & -(3\lambda + 2\mu)\alpha(T^{(0)} - T_0)\delta_{ij}\end{aligned} \tag{20}$$

$$\begin{aligned}\sigma_{ij}^{(1)} = {} & \lambda(e_{xkk}(\mathbf{u}^{(1)}) + e_{ykk}(\mathbf{u}^{(2)}))\delta_{ij} + 2\mu(e_{xij}(\mathbf{u}^{(1)}) + e_{yij}(\mathbf{u}^{(2)})) \\ & -(3\lambda + 2\mu)\alpha T^{(1)}\end{aligned} \tag{21}$$

and

$$q_j^{(-1)} = -k\frac{\partial T^{(0)}}{\partial y_j}\ ;\ q_j^{(0)} = -k(\frac{\partial T^{(0)}}{\partial x_j} + \frac{\partial T^{(1)}}{\partial y_j})\ ;\ q_j^{(1)} = -k(\frac{\partial T^{(1)}}{\partial x_j} + \frac{\partial T^{(2)}}{\partial y_j}) \tag{22}$$

The asymptotic developments of momentum and temperature equations

(2-3) lead to problems of order ε^α, with $\alpha = -2, -1, 0$, in the form :

$$\frac{\partial q_j^{(-1)}}{\partial y_j} = 0 \quad ; \quad \frac{\partial \sigma_{ij}^{(-1)}}{\partial y_j} = 0 \tag{23}$$

$$(3\lambda + 2\mu)\alpha T^{(0)} \frac{\partial e_{yij}(u^{(0)})}{\partial t} + \frac{\partial q_j^{(-1)}}{\partial x_j} + \frac{\partial q_j^{(0)}}{\partial y_j} = 0 \; ; \; \frac{\partial \sigma_{ij}^{(-1)}}{\partial x_j} + \frac{\partial \sigma_{ij}^{(0)}}{\partial y_j} = 0 \tag{24}$$

$$c\frac{\partial T^{(0)}}{\partial t} + (3\lambda + 2\mu)\alpha T^{(0)}(\frac{\partial e_{xij}(u^{(0)})}{\partial t} + \frac{\partial e_{yij}(u^{(1)})}{\partial t}) + \frac{\partial q_j^{(0)}}{\partial x_j} + \frac{\partial q_j^{(1)}}{\partial y_j} = 0 \quad ;$$

$$\frac{\partial \sigma_{ij}^{(0)}}{\partial x_j} + \frac{\partial \sigma_{ij}^{(1)}}{\partial y_j} - \rho \frac{\partial^2 u^{(0)}}{\partial x_j} = 0 \tag{25}$$

Corresponding boundary conditions are obtained from (6) for the terms of different orders $\boldsymbol{\sigma}^{(m)}$ and $\boldsymbol{q}^{(m)}$:

$$\sigma_{ij}^{(m)} N_j = 0 \quad ; \quad q_j^{(m)} N_j = 0 \qquad m = -1, 0, 1 \tag{26}$$

At the microcrack tips, a supplementary condition is given by (12) relating the energy-relase rate (7) and the heat dissipation term (10). Using the development (16) and the link between length elements in the physical and reference cells $ds = \varepsilon ds_y$, we get :

$$D^\varepsilon = D^{(0)} + \varepsilon D^{(1)} + \varepsilon^2 D^{(2)} + ... \tag{27}$$

where

$$D^{(0)} = \lim_{r\to 0} \int_{\Gamma Y_r} -k \frac{\partial T^{(0)}}{\partial y_j} n_j ds_y \; ; \; D^{(1)} = \lim_{r\to 0} \int_{\Gamma Y_r} -k(\frac{\partial T^{(0)}}{\partial x_j} + \frac{\partial T^{(1)}}{\partial y_j}) n_j ds_y$$

$$D^{(2)} = \lim_{r\to 0} \int_{\Gamma Y_r} -k(\frac{\partial T^{(1)}}{\partial x_j} + \frac{\partial T^{(2)}}{\partial y_j}) n_j ds_y \tag{28}$$

The asymptotic development of the energy release rate can be written from (7) in the form :

$$\mathcal{G}^{d\varepsilon} = \frac{1}{\varepsilon}\mathcal{G}^{(-1)} + \mathcal{G}^{(0)} + \varepsilon \mathcal{G}^{(1)} + ... \tag{29}$$

The complete expressions of the terms appearing in this relation are given in the Appendix 1. Introduction of the expansions of $\mathcal{G}^{d\varepsilon}$ and D^{ε} in the criterion (11) provides the link between different orders terms of heating dissipation and energy-release rate :

$$D^{(0)} = \frac{1}{2}\frac{dd}{dt}L_c\mathcal{G}^{(-1)} \quad ; \quad D^{(1)} = \frac{1}{2}\frac{dd}{dt}L_c\mathcal{G}^{(0)} \quad ; \quad D^{(2)} = \frac{1}{2}\frac{dd}{dt}L_c\mathcal{G}^{(1)} \tag{30}$$

At the order ε^{-2}, the problem for $\mathbf{u}^{(0)}$ and $T^{(0)}$ results from (23), (26) and (30) as :

$$\tfrac{\partial}{\partial y_j}(\lambda e_{ykk}(\mathbf{u}^{(0)})\delta_{ij} + 2\mu e_{yij}(\mathbf{u}^{(0)})) = 0 \qquad \text{in} \qquad Y \tag{31}$$

$$(\lambda e_{ykk}(\mathbf{u}^{(0)})\delta_{ij} + 2\mu e_{yij}(\mathbf{u}^{(0)}))N_j = 0 \qquad \text{on} \qquad CY \tag{32}$$

and the thermal equations

$$\frac{\partial^2 T^{(0)}}{\partial y_1^2} + \frac{\partial^2 T^{(0)}}{\partial y_2^2} = 0 \qquad \text{in} \qquad Y \tag{33}$$

$$\frac{\partial T^{(0)}}{\partial y_j}N_j = 0 \qquad \text{on} \qquad CY \tag{34}$$

$$\lim_{r\to 0}\int_{\Gamma Y_r} -k\frac{\partial T^{(0)}}{\partial y_j}n_j ds_y = \frac{1}{2}\frac{dd}{dt}L_c\mathcal{G}^{(-1)} \quad \text{at} \quad (y_1, y_2) = (\pm\frac{dL_c}{2}, 0) \tag{35}$$

In the last condition, considered at both microcrack tips in the reference cell, the term $\mathcal{G}^{(-1)}$ is given by the expression (82). Periodicity conditions are assumed on the opposite exterior boundaries of Y.

Choosing $\mathbf{u}^{(0)} = \mathbf{u}^{(0)}(\mathbf{x}, t)$ and $T^{(0)} = T^{(0)}(\mathbf{x}, t)$ independent of the y variables, we can verify the system of equations (31 - 35). They represent the macroscopic displacement and temperature fields.

The next order (ε^{-1}) problem, for $\mathbf{u}^{(1)}$ and $T^{(1)}$, can be deduced from Eqs

(24), (26) and the second relation (30) as :

$$\frac{\partial}{\partial y_j}(\lambda e_{ykk}(\mathbf{u}^{(1)})\delta_{ij} + 2\mu e_{yij}(\mathbf{u}^{(1)})) = 0 \qquad \text{in} \quad Y \tag{36}$$

$$\begin{aligned}(\lambda e_{ykk}(\mathbf{u}^{(1)})\delta_{ij} + 2\mu e_{yij}(\mathbf{u}^{(1)}))N_j = -(\lambda e_{xkk}(\mathbf{u}^{(0)})\delta_{ij} + 2\mu e_{xij}(\mathbf{u}^{(0)}) \\ -(3\lambda + 2\mu)\alpha(T^{(0)} - T_0)\delta_{ij})N_j \qquad \text{on} \quad CY\end{aligned} \tag{37}$$

and

$$\frac{\partial^2 T^{(1)}}{\partial y_1^2} + \frac{\partial^2 T^{(1)}}{\partial y_2^2} = 0 \qquad \text{in} \quad Y \tag{38}$$

$$\frac{\partial T^{(1)}}{\partial y_j}N_j = -\frac{\partial T^{(0)}}{\partial x_j}N_j \qquad \text{on} \quad CY \tag{39}$$

$$\lim_{r\to 0}\int_{\Gamma Y_r} -k(\frac{\partial T^{(0)}}{\partial x_j} + \frac{\partial T^{(1)}}{\partial y_j})n_j ds_y = \frac{1}{2}\frac{dd}{dt}L_c\mathcal{G}^{(0)} \text{ at } (y_1, y_2) = (\pm\frac{dL_c}{2}, 0) \tag{40}$$

On the external boundaries of Y periodicity conditions complete the formulation of these cell problems.

For given $\mathbf{u}^{(0)}(\mathbf{x}, t)$ and $T^{(0)}(\mathbf{x}, t)$, the solution $\mathbf{u}^{(1)}$ of (36-37) has the classical $r^{1/2}$ singularity as (y_1, y_2) approaches the crack tips. In the expression (83) of $\mathcal{G}^{(0)}$ the integrant is not singular enough to get a non-vanishing limit, such that the right member of (40) is equal to 0.

The particular form of the boundary condition (37) shows that the general solution of (36-37), for the first-order corrector $\mathbf{u}^{(1)}$, is of the form :

$$\mathbf{u}^{(1)}(\mathbf{x}, \mathbf{y}, t) = \boldsymbol{\xi}^{pq}(\mathbf{y})e_{xpq}(\mathbf{u}^{(0)})(\mathbf{x}, t) + \boldsymbol{\phi}(\mathbf{x}, t)(T^{(0)} - T_0) \tag{41}$$

Here the characteristic functions $\boldsymbol{\xi}^{pq}$ are obtained by solving the unit-cell problem :

$$\frac{\partial}{\partial y_j}(\lambda e_{ykk}(\boldsymbol{\xi}^{pq})\delta_{ij} + 2\mu e_{yij}(\boldsymbol{\xi}^{pq})) = 0 \qquad \text{in} \quad Y \tag{42}$$

$$(\lambda e_{ykk}(\boldsymbol{\xi}^{pq})\delta_{ij} + 2\mu e_{yij}(\boldsymbol{\xi}^{pq}))N_j = -(\lambda\delta_{ij}\delta_{pq} + \mu(\delta_{ip}\delta_{jq} + \delta_{iq}\delta_{jp}))N_j \text{ on } CY \tag{43}$$

while $\boldsymbol{\phi}$ is the solution of the second problem :

$$\frac{\partial}{\partial y_j}(\lambda e_{ykk}(\boldsymbol{\phi})\delta_{ij} + 2\mu e_{yij}(\boldsymbol{\phi})) = 0 \qquad \text{in} \quad Y \tag{44}$$

$$(\lambda e_{ykk}(\boldsymbol{\phi})\delta_{ij} + 2\mu e_{yij}(\boldsymbol{\phi}))N_j = (3\lambda + 2\mu)\alpha\delta_{ij}N_j \qquad \text{on} \quad CY \tag{45}$$

The temperature corrector $T^{(1)}$ is obtained from (38-40) and depends linearly on the right member of (39), with $N_1 = 0$, $N_2 = 1$:

$$T^{(1)}(\mathbf{x}, \mathbf{y}, t) = \theta(\mathbf{y})\frac{\partial T^{(0)}}{\partial x_2}(\mathbf{x}, t) \tag{46}$$

where θ is solution of the following unit cell problem :

$$\frac{\partial^2\theta}{\partial y_1^2} + \frac{\partial^2\theta}{\partial y_2^2} = 0 \qquad \text{in} \quad Y \tag{47}$$

$$\frac{\partial\theta}{\partial y_2} = -1 \qquad \text{on} \quad CY \tag{48}$$

$$\lim_{r\to 0}\int_{\Gamma Y_r}\frac{\partial\theta}{\partial y_j}n_j ds_y = 0 \quad \text{at} \quad (y_1, y_2) = (\pm\frac{dL_c}{2}, 0) \tag{49}$$

We note that the solutions of the unit cell problems (42-43), (44-45) and (47-49) depend on the normalized microcrack length d.

At the order ε^0, we get the following problems for thermal and displacement fields :

$$k(\frac{\partial^2 T^{(0)}}{\partial x_1^2} + \frac{\partial^2 T^{(0)}}{\partial x_2^2} + 2(\frac{\partial^2 T^{(1)}}{\partial x_1\partial y_1} + \frac{\partial^2 T^{(1)}}{\partial x_2\partial y_2}) + \frac{\partial^2 T^{(2)}}{\partial y_1^2} + \frac{\partial^2 T^{(2)}}{\partial y_2^2})$$
$$-(3\lambda + 2\mu)\alpha T^{(0)}\frac{\partial}{\partial t}(e_{x11}(\mathbf{u}^{(0)}) + e_{x22}(\mathbf{u}^{(0)})$$
$$+e_{y11}(\mathbf{u}^{(1)}) + e_{y22}(\mathbf{u}^{(1)})) = c\frac{\partial T^{(0)}}{\partial t} \quad \text{in } Y \tag{50}$$

$$\frac{\partial T^{(1)}}{\partial x_2} + \frac{\partial T^{(2)}}{\partial y_2} = 0 \text{ on } \quad CY \tag{51}$$

$$\lim_{r\to 0}\int_{\Gamma Y_r} -k(\frac{\partial T^{(1)}}{\partial x_j} + \frac{\partial T^{(2)}}{\partial y_j})n_j ds_y = \frac{1}{2}\frac{dd}{dt}L_c\mathcal{G}^{(1)} \text{ at } (y_1, y_2) = (\pm\frac{dL_c}{2}, 0) \tag{52}$$

and

$$\frac{\partial}{\partial x_j}(\lambda(e_{xkk}(\mathbf{u}^{(0)})+e_{ykk}(\mathbf{u}^{(1)}))\delta_{ij}+2\mu(e_{xij}(\mathbf{u}^{(0)})+e_{yij}(\mathbf{u}^{(1)}))$$
$$-(3\lambda+2\mu)\alpha(T^{(0)}-T_0)\delta_{ij})+\frac{\partial}{\partial y_j}(\lambda(e_{xkk}(\mathbf{u}^{(1)})+e_{ykk}(\mathbf{u}^{(2)}))\delta_{ij}$$
$$+2\mu(e_{xij}(\mathbf{u}^{(1)})+e_{yij}(\mathbf{u}^{(2)}))-(3\lambda+2\mu)\alpha T^{(1)}\delta_{ij})=\rho\frac{\partial^2\mathbf{u}_i^{(0)}}{\partial t^2}\ \text{ in } Y \quad (53)$$
$$(\lambda(e_{xkk}(\mathbf{u}^{(1)})+e_{ykk}(\mathbf{u}^{(2)}))\delta_{ij}+2\mu(e_{xkk}(\mathbf{u}^{(1)})+e_{yij}(\mathbf{u}^{(2)}))$$
$$-(3\lambda+2\mu)\alpha T^{(1)}\delta_{ij})N_j=0\ \text{ on } CY \quad (54)$$

In order to deduce the effective thermo-mechanical balance laws we apply the mean value operator $\langle\cdot\rangle=(1/|Y|)\int_Y\cdot\,dy$, with $|Y|={L_c}^2$ the area of Y, to (50) and (53). Integration by parts, use of the periodicity conditions and the crack-tip relations of the form (52) lead to :

$$c^{eff}\frac{\partial T^{(0)}}{\partial t}+T^{(0)}\beta_{ij}^{eff}\frac{\partial e_{xij}(\mathbf{u}^{(0)})}{\partial t}+\frac{\partial Q_i^{(0)}}{\partial x_i}=\frac{\mathcal{G}^{(1)}}{L_c}\frac{dd}{dt} \quad (55)$$

$$\rho^{eff}\frac{\partial^2\mathbf{u}_i^{(0)}}{\partial t^2}-\frac{\partial\Sigma_{ij}^{(0)}}{\partial x_j}=0 \quad (56)$$

where the macroscopic stress $\Sigma_{ij}^{(0)}=\langle\sigma_{ij}^{(0)}\rangle$ and heat flux $Q_i^{(0)}=\langle q_i^{(0)}\rangle$ are given by

$$\Sigma_{ij}^{(0)} = C_{ijkl}^{eff}e_{xkl}(\mathbf{u}^{(0)})-\varphi_{ij}^{eff}(T^{(0)}-T_0) \quad (57)$$
$$Q_i^{(0)} = -k_{ij}^{eff}\frac{\partial T^{(0)}}{\partial x_j} \quad (58)$$

As concerns the expressions of the homogenized coefficients, we obtain for the effective specific heat coefficient :

$$c^{eff}=c+T^{(0)}S^* \quad (59)$$

with the thermal modulus S^* given by

$$S^* = \frac{1}{|Y|}\int_Y (3\lambda + 2\mu)\alpha(e_{y11}(\boldsymbol{\phi}) + e_{y22}(\boldsymbol{\phi}))dy \tag{60}$$

The effective elastic moduli C_{ijkl}^{eff} are computed with the cell solutions as :

$$C_{ijkl}^{eff} = \frac{1}{|Y|}\int_Y \left(\lambda\delta_{ij}\delta_{kl} + \mu(\delta_{ik}\delta_{jl} + \delta_{il}\delta_{jk}) + \lambda e_{ymm}(\boldsymbol{\xi}^{kl})\delta_{ij} + 2\mu e_{yij}(\boldsymbol{\xi}^{kl})\right) dy \tag{61}$$

and the homogenized mass density :

$$\rho^{eff} = \frac{1}{|Y|}\int_Y \rho dy \tag{62}$$

For the thermal expansion coefficients we obtain the formulae

$$\beta_{ij}^{eff} = \frac{1}{|Y|}\int_Y \alpha(3\lambda + 2\mu)(\delta_{ij} + e_{ymm}(\boldsymbol{\xi}^{ij}))dy \tag{63}$$

$$\varphi_{ij}^{eff} = \frac{1}{|Y|}\int_Y (\alpha(3\lambda + 2\mu)\delta_{ij} - C_{ijkl}e_{ykl}(\boldsymbol{\phi}))dy \tag{64}$$

and we prove the equality $\beta_{ij}^{eff} = \varphi_{ij}^{eff}$ using the corresponding cell problems for the characteristic functions.

The homogenized thermal conduction components are :

$$k_{11}^{eff} = \frac{1}{|Y|}\int_Y k dy \ ; \ k_{12}^{eff} = \frac{1}{|Y|}\int_Y k\frac{\partial\theta}{\partial y_1}dy \ ; \ k_{22}^{eff} = \frac{1}{|Y|}\int_Y k(1 + \frac{\partial\theta}{\partial y_2})dy \tag{65}$$

We remark that the effective coefficients S^*, C_{ijkl}^{eff}, φ_{ij}^{eff} and k_{ij}^{eff} depend on the damage variable d. This dependence will be illustrated numerically in Section 5 for a particular set of initial material constants and different microcrack lengths.

As concerns the homogenized temperature equation (55), the development in the next section will allow us to express the right member as a fully macroscopic dissipation term.

4. Dynamic damage evolution

In order to obtain a complete thermoelastic damage problem, we have to supplement the equations (55-58) with an evolution equation for the damage variable $d(x_i, t)$. Based on previous contributions (Dascalu et al., 2008; Keita et al., 2014; Dascalu, 2018), we develop in this Section a microfracture-to-damage homogenization approach in the non-classical framework of dynamic thermo-elastic fracture with heat production. In the particular case when the heating term in the right of (55) is neglected, the final product of this Section will be a new thermo-elastic damage law in dynamics.

An energy analysis will be performed with the solutions of the cell problems formulated in the previous section, in the case of propagating microcracks. We will assume that, in the reference cell Y, the crack CY of length $d(t).L_c$ extends symmetrically, the two tips moving with the velocity $\frac{1}{2}\frac{dd}{dt}.L_c$. In order to properly account for the singularity of the fields and the energy flow at microcrack tips during this evolution, we will first work on the domain Y_r representing the cell Y without the interiors of the cercles ΓY_r^g and ΓY_r^d (see Fig. 2). We also denote by CY_r the part of the crack line inside Y_r. The fields defined on Y with the crack CY will then be recovered by taking the limit $r \to 0$.

Multiplication of the equation (36) by $\dot{u}_i^{(1)}$, integration on Y_r, use of perio-

dicity conditions and Reynolds transport theorem lead to the energy balance :

$$\frac{d}{dt}\int_{Y_r}\frac{1}{2}C_{ijkl}e_{ykl}(\mathbf{u}^{(1)})e_{yij}(\mathbf{u}^{(1)})dy$$
$$+\int_{\Gamma Y_r^g\cup\Gamma Y_r^d}\left(\frac{1}{2}C_{ijkl}e_{ykl}(\mathbf{u}^{(1)})e_{yij}(\mathbf{u}^{(1)})\frac{1}{2}\frac{dd}{dt}L_c n_1+C_{ijkl}e_{ykl}(\mathbf{u}^{(1)})n_j\dot{u}_i^{(1)}\right)ds_y$$
$$=\int_{CY_r}C_{ijkl}e_{ykl}(\mathbf{u}^{(1)})N_j\left[\dot{u}_i^{(1)}\right]ds_y \qquad (66)$$

where we have used the compact notation $C_{ijkl}=\lambda\delta_{ij}\delta_{kl}+\mu(\delta_{ik}\delta_{jl}+\delta_{il}\delta_{jk})$ for the initial elastic coefficients. The brackets $[f]=f^+-f^-$ denote the jump of f over the crack faces, with the $+$ value on the side given by the orientation of the normal vector $\mathbf{N}$, as illustrated in Fig. 2.

The singularity of field $\dot{u}_i^{(1)}$ allows us (Freund, 1990; Bui et al., 1980) to use the local relation $\dot{u}_i^{(1)}\simeq-\frac{1}{2}\frac{dd}{dt}L_c\frac{\partial u_i^{(1)}}{\partial y_1}$ in the vicinity of the crack tips. In this way, by taking the limit we retrieve the energy-release rate term $\mathcal{G}^{(1)}$, given in (88), for the two crack tips and the previous relation becomes :

$$\frac{d}{dt}\int_{Y}\frac{1}{2}C_{ijkl}e_{ykl}(\mathbf{u}^{(1)})e_{yij}(\mathbf{u}^{(1)})dy+\frac{dd}{dt}L_c\mathcal{G}^{(1)}$$
$$=\int_{CY}C_{ijkl}e_{ykl}(\mathbf{u}^{(1)})N_j\left[\dot{u}_i^{(1)}\right]ds_y \qquad (67)$$

A similar procedure can be applied starting with the equation (31) in the slightly modified form

$$\frac{\partial}{\partial y_j}\left(C_{ijkl}e_{xkl}(\mathbf{u}^{(0)})-\beta T^{(0)}\delta_{ij}\right)=0$$

with $\beta=\alpha(3\lambda+2\mu)$. Using the fact that $\mathbf{u}^{(0)}$ and $T^{(0)}$ do not depend on y_i variables, we obtain :

$$\int_Y(C_{ijkl}e_{xkl}(\mathbf{u}^{(0)})-\beta T^{(0)}\delta_{ij})e_{yij}(\dot{\mathbf{u}}^{(1)})dy$$
$$-\int_{CY}(C_{ijkl}e_{xkl}(\mathbf{u}^{(0)})-\beta T^{(0)}\delta_{ij})N_j[\dot{u}_i^{(1)}]ds_y=0 \qquad (68)$$

Combining (67) and (68) and using the boundary condition (37) on the crack faces allow us to obtain

$$\frac{d}{dt}\int_Y \frac{1}{2}C_{ijkl}e_{ykl}(\mathbf{u}^{(1)})e_{yij}(\mathbf{u}^{(1)})dy + \int_Y (C_{ijkl}e_{xkl}(\mathbf{u}^{(0)}) - \beta T^{(0)}\delta_{ij})e_{yij}(\dot{\mathbf{u}}^{(1)})dy$$
$$+\frac{dd}{dt}L_c\mathcal{G}^{(1)} = -\int_{CY}(\beta T_0\delta_{ij})N_j[\dot{u}_i^{(1)}]ds_y = -\frac{d}{dt}\int_Y \beta T_0\delta_{ij}e_{yij}(\mathbf{u}^{(1)})dy \qquad (69)$$

where the last equality results by integration of $\frac{\partial}{\partial y_j}(\alpha(\beta T_0\delta_{ij}) = 0$.

In the second term of (69) we can interchange the time derivative so that to obtain the equivalent identity :

$$\frac{1}{2}\frac{d}{dt}\int_Y (C_{ijkl}(e_{xkl}(\mathbf{u}^{(0)}) + e_{ykl}(\mathbf{u}^{(1)})) - \beta(T^{(0)} - T_0))e_{yij}(\mathbf{u}^{(1)})dy$$
$$+\frac{1}{2}\frac{d}{dt}\int_Y (C_{ijkl}e_{xkl}(\mathbf{u}^{(0)}) - \beta(T^{(0)} - T_0))e_{yij}(\mathbf{u}^{(1)})dy + \frac{dd}{dt}L_c\mathcal{G}^{(1)}$$
$$= \int_Y (C_{ijkl}e_{xkl}(\dot{\mathbf{u}}^{(0)}) - \beta\dot{T}^{(0)}\delta_{ij})e_{yij}(\mathbf{u}^{(1)})dy \qquad (70)$$

On the other hand, if the equation (36) in its equivalent form

$$\frac{\partial}{\partial y_j}\left(C_{ijkl}(e_{xkl}(\mathbf{u}^{(0)}) + e_{ykl}(\mathbf{u}^{(1)})) - \beta(T^{(0)} - T_0)\delta_{ij}\right) = 0$$

is multiplied by u_i and integrated over Y, and the crack face conditions (37) are used, we get :

$$\int_Y \left(C_{ijkl}(e_{xkl}(\mathbf{u}^{(0)}) + e_{ykl}(\mathbf{u}^{(1)})) - \beta(T^{(0)} - T_0)\delta_{ij}\right)e_{yij}(\mathbf{u}^{(1)})dy = 0 \qquad (71)$$

With this last relation the identity (69) reduces to

$$\frac{dd}{dt}L_c\mathcal{G}^{(1)} = \int_Y C_{ijkl}e_{ykl}(\mathbf{u}^{(1)})dy\, e_{xij}(\dot{\mathbf{u}}^{(0)}) - \int_Y \beta e_{ykl}(\mathbf{u}^{(1)})\delta_{kl}dy\,\dot{T}^{(0)}$$
$$-\frac{1}{2}\frac{d}{dt}\int_Y C_{ijkl}e_{ykl}(\mathbf{u}^{(1)})dy\, e_{xij}(\mathbf{u}^{(0)}) + \frac{1}{2}\frac{d}{dt}\int_Y \beta e_{ykl}(\mathbf{u}^{(1)})\delta_{kl}dy\,(T^{(0)} - T_0) \qquad (72)$$

In order to evaluate the integrals in the right member of (72) we use the particular structure (41) of the first order corrector $\mathbf{u}^{(1)}$ together with the

expressions (61), (63) and (60) of the effective coefficients C_{ijmn}^{eff}, β_{ij}^{eff} and S^*, respectively. We obtain in this way :

$$\int_Y C_{ijkl} e_{ykl}(\mathbf{u}^{(1)}) dy = {L_c}^2((C_{ijmn}^{eff} - C_{ijmn}) e_{xmn}(\mathbf{u}^{(0)}) - (\beta_{ij}^{eff} - \beta\delta_{ij})(T^{(0)} - T_0)) \quad (73)$$

$$\int_Y \beta e_{ykl}(\mathbf{u}^{(1)}) \delta_{kl} dy = {L_c}^2((\beta_{ij}^{eff} - \beta\delta_{ij}) e_{xij}(\mathbf{u}^{(0)}) + S^*(T^{(0)} - T_0)) \quad (74)$$

With these expressions replaced in (72) we finally obtain

$$\frac{dd}{dt}(\frac{\mathcal{G}^{(1)}}{L_c} + \frac{1}{2}\frac{dC_{ijkl}^{eff}}{dd} e_{xkl}(\mathbf{u}^{(0)}) e_{xij}(\mathbf{u}^{(0)}) - \frac{d\beta_{ij}^{eff}}{dd}(T^{(0)} - T_0) e_{xij}(\mathbf{u}^{(0)}) - \frac{1}{2}\frac{dS^*}{dd}(T^{(0)} - T_0)^2) = 0 \quad (75)$$

For evolving microcracks ($\frac{dd}{dt} \neq 0$), the last relation establishes a link between the first-order energy-release rate term $\mathcal{G}^{(1)}$ and the macroscopic quantity :

$$\mathcal{Y} = -\frac{1}{2}\frac{dC_{ijkl}^{eff}}{dd} e_{xkl}(\mathbf{u}^{(0)}) e_{xij}(\mathbf{u}^{(0)}) + \frac{d\beta_{ij}^{eff}}{dd}(T^{(0)} - T_0) e_{xij}(\mathbf{u}^{(0)}) + \frac{1}{2}\frac{dS^*}{dd}(T^{(0)} - T_0)^2 \quad (76)$$

which represents the volumetric density of damage energy release rate.

Used in combination with a microscopic crack propagation criterion, the equation (75) provides the macroscopic damage law. Consider a Griffith type criterion $\mathcal{G}^{d\varepsilon} = \mathcal{G}_c$, with $\mathcal{G}_c(v_p)$ the critical fracture energy that may depend on the crack speed $v_p = \frac{l_c}{2}\frac{dd}{dt}$. For rapid propagation it may be showed (Freund, 1990; Ravi-Chandar, 2004) that

$$\mathcal{G}^{d\varepsilon} = g(v_p)\mathcal{G}^{\varepsilon} \simeq (1 - \frac{v_p}{C_R})\mathcal{G}^{\varepsilon} \quad (77)$$

where $g(v_p)$ is a universal function of the crack speed that may be approximated, for mode I propagation, by $g(v_p) \simeq 1 - \frac{v_p}{C_R}$. Here C_R is the Rayleigh wave velocity and the quantity $\mathcal{G}^{\varepsilon}$ is the instantaneous quasi-static energy release rate corresponding to a given microcrack length.

The asymptotic development (87-89) of $\mathcal{G}^{d\varepsilon}$ given in the Appendix show the link with the quasi-static energy release rate : $\mathcal{G}^{\varepsilon} = \varepsilon \mathcal{G}^{(1)}$. As remarked in the Appendix, the development (87) is incomplete in the sense that it corresponds to the approximation given by the consideration of only the first order correctors. A better solution for capturing the dynamic effects is to use the expression (77) of $\mathcal{G}^{d\varepsilon}$ together with $\mathcal{G}^{\varepsilon} = \varepsilon \mathcal{G}^{(1)}$, as proposed in Dascalu (2018) for the purely elastic case. In this way, we have $\mathcal{G}^{d\varepsilon} = \varepsilon g(v_p) \mathcal{G}^{(1)}$ and we can write (75) in the form :

$$\frac{dd}{dt}\left(\frac{\mathcal{G}_c(v_p)}{\varepsilon g(v_p) L_c} - \mathcal{Y}\right) = 0 \tag{78}$$

As a linear approximation of the crack-speed dependent fracture energy (e.g., Bjerke and Lambros, 2003; Dalmas et al., 2013), we consider $\mathcal{G}_c(v_p) = \mathcal{G}_{c0}(1 + a.v_p)$ with constant parameters $\mathcal{G}_{c0}$ and a. In this case, the use of the expression of the velocity $v_p = \frac{l_c}{2}\frac{dd}{dt}$ leads to the following damage evolution law :

$$\frac{dd}{dt} = \frac{2C_R}{l_c}\left\langle 1 - \frac{\mathcal{G}_{c0}(1 + aC_R)}{l_c \mathcal{Y} + aC_R \mathcal{G}_{c0}}\right\rangle \tag{79}$$

where $\langle . \rangle$ represents the positive part. We note that the microstructural length l_c is present in the equation (79).

It is important to note that, in order to incorporate realistic effects related to the velocity dependence of the energy of fracture, in the damage law (79) we considered the microscopic fracture energy $\mathcal{G}_c(v_p)$ as a function of the microcrack speed. As observed by Sharon et al. (1996, 1999), the crack-speed dependency of the fracture energy is the results of micro-branching effects requiring larger energy for the propagation of the multi-crack system. In a perfect two-scale description, evolving multi-crack systems should be

incorporated at the small scale. However, this would lead to insurmontable difficulties related to the energetic description of the arrest of the branches together with the propagation of the main microcrack, to the speed influence on the geometry of the multi-crack system producing damage-rate dependent effective coefficients and making difficult the obtention of the damage evolution law or to the non-uniqueness of the cell solutions related to micro-branching instabilities and compromising the well-definiteness of the homogenized response. To avoid all these difficulties, we proposed a relatively simple solution to incorporate the velocity effects in the damage law. This allowed us to rigorously obtain the damage evolution law by homogenization and, as we will see in the last section, to have good agreements between the model predictions and the experimental results.

The damage energy-release rate $\mathcal{Y}$ is calculated with the displacement and temperature fields such that (79) forms with the equations (55-58) a coupled thermoelastic and damage system. In order to obtain the temperature equation in a completely macroscopic form, we should replace the expression of

$$\mathcal{G}^{(1)} = \frac{\mathcal{G}_{c0}(1 + a.v_p)}{\varepsilon g(v_p)} = \frac{\mathcal{G}_{c0} L_c C_R (2 + a.l_c \frac{dd}{dt})}{l_c (2C_R - l_c \frac{dd}{dt})}$$

In this way (55) becomes :

$$c^{eff} \frac{\partial T^{(0)}}{\partial t} + T^{(0)} \beta_{ij}^{eff} \frac{\partial e_{xij}(\mathbf{u}^{(0)})}{\partial t} + \frac{\partial Q_i^{(0)}}{\partial x_i} = \frac{\mathcal{G}_{c0} C_R (2 + a.l_c \frac{dd}{dt})}{l_c (2C_R - l_c \frac{dd}{dt})} \frac{dd}{dt} \qquad (80)$$

as the macroscopic temperature equation in which the right member source term represents the damage dissipation as heat.

Finally, we note that the expression of the heat production term in the equation (80) is the consequence of the particular expressions considered for

$g(v_p)$ and $\mathcal{G}_c(v_p)$. The general form of the right member in the macroscopic temperature equation is $\frac{\mathcal{G}_c(\frac{l_c}{2}\frac{dd}{dt})}{l_c g(\frac{l_c}{2}\frac{dd}{dt})}\frac{dd}{dt}$. For the examples given in the next sections the particular expression (80) is adopted.

5. Local macroscopic response

The objective of this section is the study of the local macroscopic behavior predicted by the new damage model. We first analyse the effective coefficients as functions of the damage variable using interpolations of their numerical values computed with the numerical solutions of the cell problems for a number of microcrack lengths. Then we illustrate the local macroscopic response of the model for uniaxial loadings with special emphasis on the influence of microscopic dissipation as heat, the loading rate, the size of the microstructure and the initial damage value.

The material parameters used for the computations correspond to a PMMA polymer : the dynamic Young modulus $E = 5\,GPa$, the Poisson ratio $\nu = 0.37$, the mass density $\rho = 1180\,kg.m^{-3}$, the thermal expansion coefficient $\alpha = 10^{-4}K^{-1}$, the heat capacity $c = 10^6\,J.m^{-3}.K^{-1}$ and the thermal conductivity $k = 0.2\,W.m^{-1}.K^{-1}$.

For the fracture energy, we adopt the approximation given in the previous section $\mathcal{G}_c(v_p) = \mathcal{G}_{c0}(1+a.v_p)$ with $\mathcal{G}_{c0} = 400\,J.m^{-2}$ and $a = 0.025\,s.m^{-1}$. This choice of parameters is consistent with the values of the fracture energy at different crack tip speeds reported in the literature (e.g., Bjerke and Lambros, 2003; Dalmas et al., 2013) for PMMA polymers.

5.1. Homogenized coefficients

The effective coefficients are calculated with the formulae (59-65) using the characteristic functions ξ^{pq}, ϕ and θ that are solutions of the cell problems (42-43), (44-45) and (47-49), respectively.

For 11 values of the normalized microcrack length $d \in [0, 1]$, these characteristic functions are computed numerically with the Finite Element method, using the FEM software COMSOL Multiphysics. The corresponding numerical values of the effective coefficients are then interpolated with polynomial functions of the damage variable. In the extreme case of a completely broken cell ($d = 1$), analytical solutions of the cell problems can be obtained and used for to calculate the effective coefficients at failure limit.

In Figure 3 the homogenized elastic coefficients $C^{eff}_{ijkl}(d)$ are represented versus the damage variable d. They are normalized with those for $d = 0$, corresponding to the virgin material. Both the discrete numerical values, computed with the finite element solutions, and the interpolation curves are shown.

While the solid matrix is assumed to be isotropic, corresponding to the effective elastic coefficients $C^{eff}_{ijkl}(0)$, the presence of microcracks induces an orthotropic effective response. The effective coefficients have a nonlinear dependence on the damage variable, with a more abrupt loss of rigidity when approaching the limit state $d = 1$. At failure, when the crack completely separates the cell into two distinct parts, vanishing response is obtained for loadings in the normal direction, given by the coefficients C^{eff}_{2222} and C^{eff}_{1122}, and in shear loadings by C^{eff}_{1212}. Only partial degradation is obtained in the response to loadings parallel to the crack direction, as observed for $C^{eff}_{1111}(d)$.

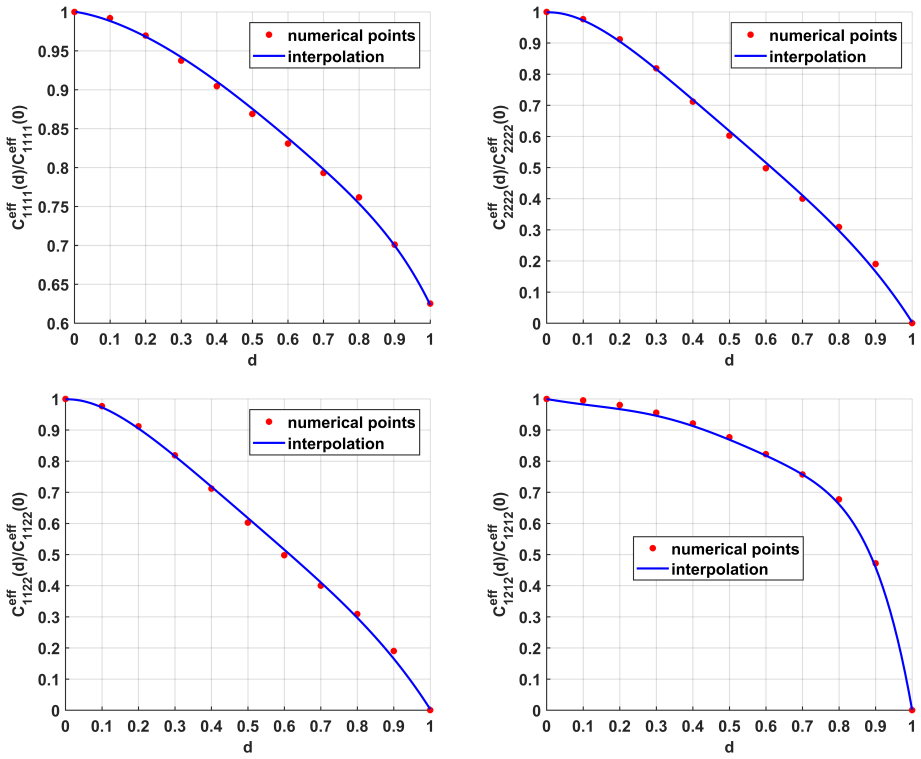

FIGURE 3: Homogenized coefficients C^{eff}_{ijkl} versus the damage variable d : computed values and interpolation curves.

Analytical solution calculations allow us to obtain the expression of the coefficient $C^{eff}_{1111}(1) = \frac{E}{1-\nu^2}$ for a completely fractured cell. This corresponds to the last point value in Figure 3.

The effective stress-temperature moduli β^{eff}_{ij} are represented in Figure 4. With the increase of the damage value, the upper and lower parts a cell are progressively separated by a traction-free and thermally isolating crack and the thermo-mechanical coupling is reduced. In particular, as a consequence of the microcrack orientation, the coefficient β^{eff}_{22} is vanishing at the complete

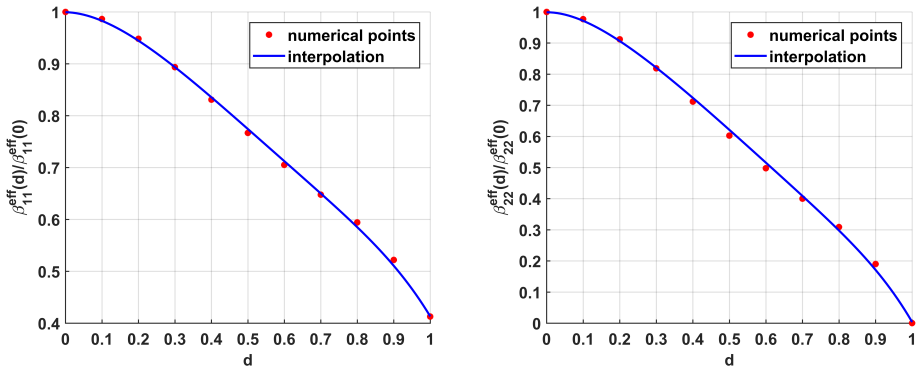

FIGURE 4: Effective stress-temperature moduli β_{11}^{eff} and β_{22}^{eff} versus damage.

failure limit. As expected, the thermal expansion is less affected in the direction of the crack line. In fact, the analytical solution of the cell problem for $d = 1$ gives the expression $\beta_{11}^{eff}(1) = \frac{E\alpha}{1-\nu}$ for this non-vanishing coefficient.

As concerns the thermal modulus S^*, that appears in the expression of the effective specific heat $c^{eff} = c + T^{(0)}S^*$, it is represented in the left side of the Figure 5 as function of damage variable. The virgin material ($d = 0$) has the heat capacity c, while for a given $d \neq 0$ the effective specific heat is increasing with the increase of S^*. The presence of a thermally isolating crack in the cell determine the necessity of more heating to increase the temperature with a unit value. At $d = 1$ we determine the analytical expression $S^*(1) = E\alpha^2\frac{1+\nu}{(1-2\nu)(1-\nu)}$ provided by the analytical solution of the problem (44-45).

On the right side of Figure 5 the effective thermal conduction coefficient $k_{22}^{eff}(d)$ is represented vs the damage value. The virgin material has isotropic conductivities $k_{11}^{eff}(0) = k$, $k_{22}^{eff}(0) = k$ and $k_{12}^{eff}(0) = 0$, while the presence of a crack induces anisotropy by reduction of $k_{22}^{eff}(d)$ and a constant conductivity $k_{11}^{eff}(d) = k$. This is the consequence of the thermally isolating

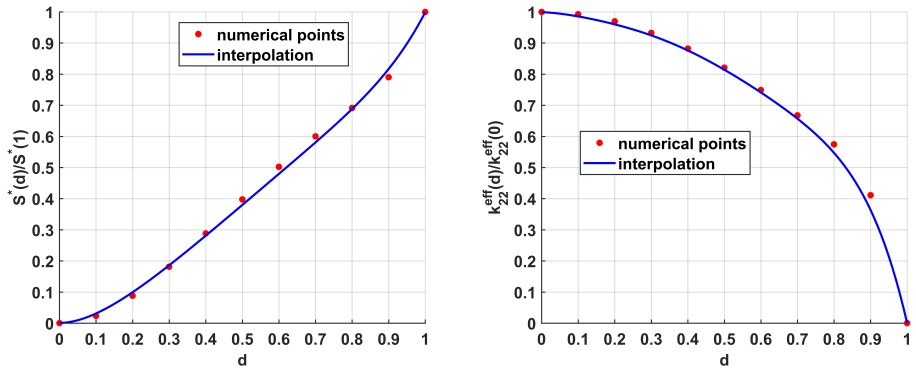

FIGURE 5: Effective thermal modulus $S^*(d)$ and conductivity coefficient $k_{22}^{eff}(d)$.

crack-face conditions. For larger values of d the overall conductivity in the direction normal to the crack is decreasing to $k_{22}^{eff}(1) = 0$, corresponding to isolating a crack traversing completely the cell.

5.2. Local response analysis

In order to analyse the homogenized response of the new damage model, we impose a strain history $e_{x22}(u^{(0)})(t)$, with constant strain rate $\dot{e}_{x22}$, as the only non-vanishing strain component. Under this loading, we determine the local response of the model in effective stress, damage and temperature by solving the the equations (79) and (80). For the description of rapid failure phenomena, we assume adiabatic conditions at the macroscopic level by neglecting the conduction term in (80). In this case, we have a coupled system of nonlinear differential equations for $T^0(t)$ and $d(t)$ that is solved numerically using a forward Euler finite-difference scheme.

Unless specified, the material parameters are those given in the beginning of this section. The initial temperature is $T_0 = 20\,^\circ C$, $d_0 = 0.1$ and the strain

rate value is $\dot{e}_{x22} = 5000\ s^{-1}$. The interpolated effective coefficients are used in the computations.

5.2.1. Influence of the heat sources

We first analyse the influence of heating during damage evolution. The temperature equation (80) is solved with and without the right member, together with the damage evolution law (79).

The obtained temperatures are plotted in Figure 6 versus the applied strain $e_{x22}(u^{(0)})$. The results are presented for three values of the microstructural length : $l_c = 10^{-4}\,m$; $l_c = 10^{-5}\,m$ and $l_c = 10^{-6}\,m$. The continuous lines represent the temperature $T^{(0)}$ when the crack-tip dissipation as heat is taken into account, while the dotted line corresponds to temperature evolutions without heating sources.

In the first stage, when the crack propagation has not been activated, we note a cooling effect, identical for the two models. This is in accordance with the experimental observations (e.g., Rittel, 1999; Bougaut and Rittel, 2001) reporting temperature decrease near the crack tip during the initiation phase of dynamic fracture and will be discussed in the next section where such an experiment will be reproduced numerically.

Once the propagation starts, the crack-tip heating is activated and influences the evolution of $T^{(0)}$ which is increasing. When the heating term is neglected, the temperature is still decreasing during microcrack growth. For smaller sizes of the microstructure, the increase of the temperature is more important and more rapid. As will be observed in the next example, in this case the microcrack propagation is more rapid leading to higher dissipation rates at the tips and the temperature can thus increase up to a few hundreds

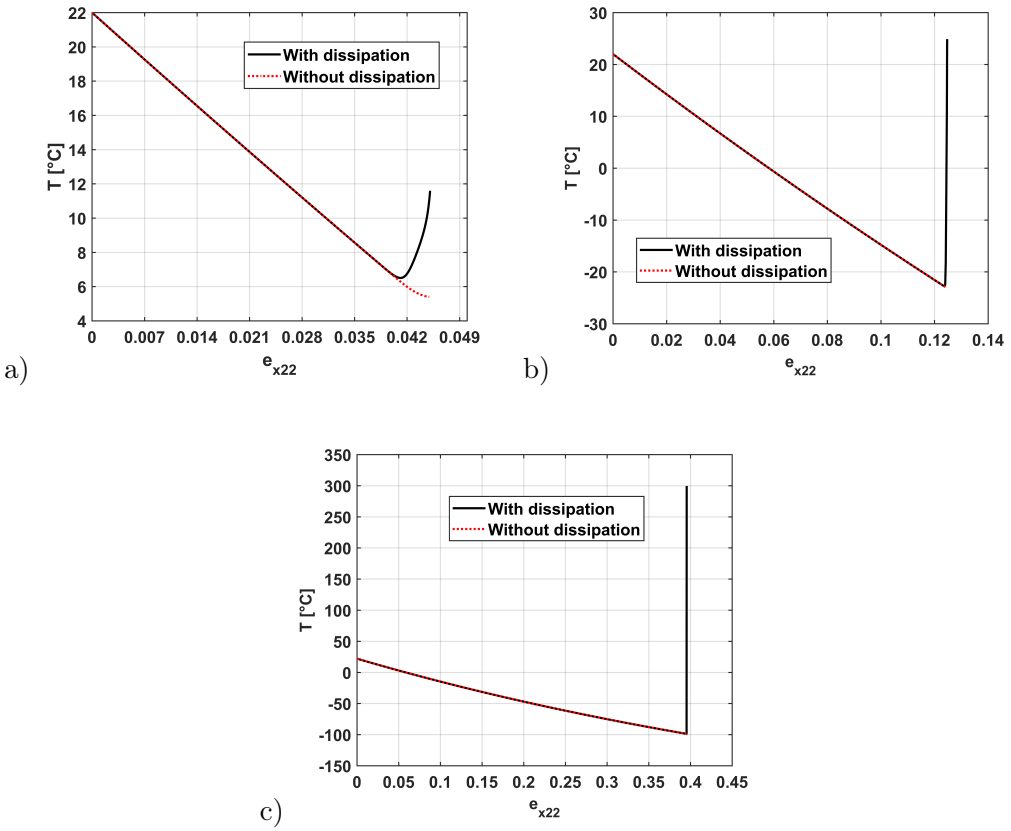

FIGURE 6: Temperature $T^{(0)}$ versus the applied strain $e_{x22}(u^{(0)})(t)$, for three sizes of the microstructure : a) $l_c = 10^{-4}\, m$; b) $l_c = 10^{-5}\, m$; c) $l_c = 10^{-6}\, m$. Evolutions with (continuous line) or without (dotted line) crack tip heating.

of degrees.

5.2.2. Influence of the microstructural size l_c

To get more insight on the influence of the microstructural length l_c on the thermo-mechanical response of the model, we represent in Figure 7 the macroscopic stress $\Sigma_{22}^{(0)}$, damage variable d and temperature $T^{(0)}$ versus the applied strain $e_{x22}(u^{(0)})$, for three lengths : $l_c = 5 \times 10^{-4}\, m$; $l_c = 5 \times 10^{-5}\, m$

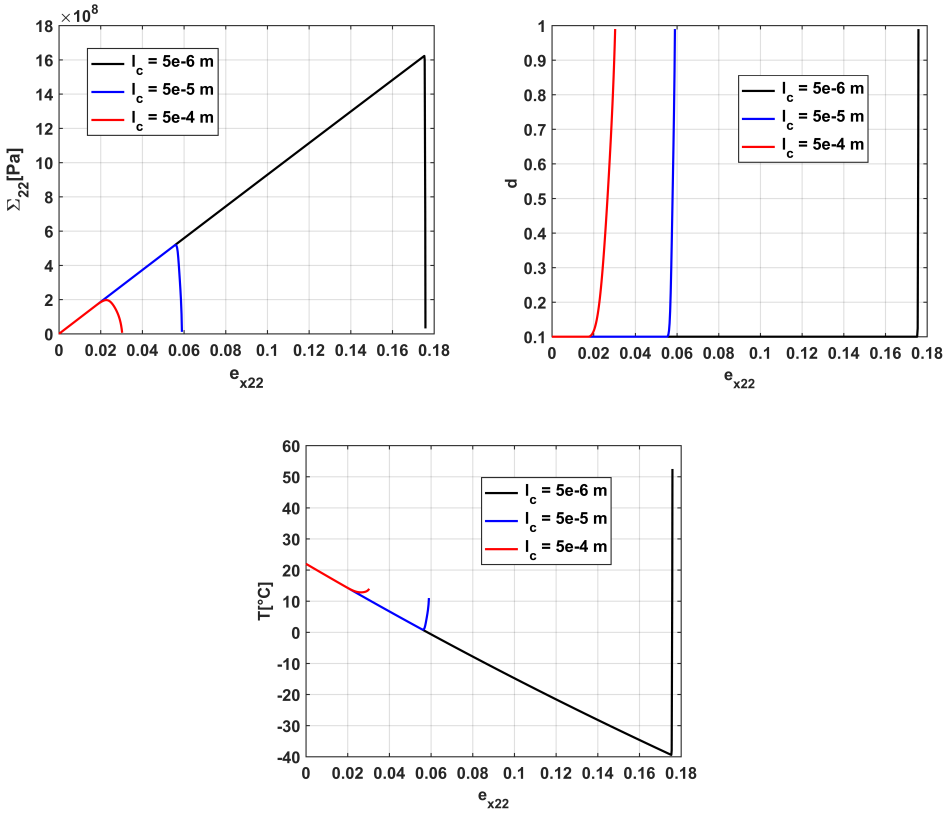

FIGURE 7: Influence of size of the microstructure on the effective stress, damage and temperature for : $l_c = 5 \times 10^{-4}\, m$; $l_c = 5 \times 10^{-5}\, m$; $l_c = 5 \times 10^{-6}\, m$.

and $l_c = 5 \times 10^{-6}\, m$.

Fine microstructures are more resistant to damage initiation since smaller microcracks are more difficult to propagate. It can be observed that, once the propagation initiated, the response of large microstructures is more ductile. This is the consequence of the fact that, for larger periods, a larger part of the supplied energy is stored as kinetic and elastic energy in the vicinity of the microcrack lips during propagation such that a smaller amount of energy

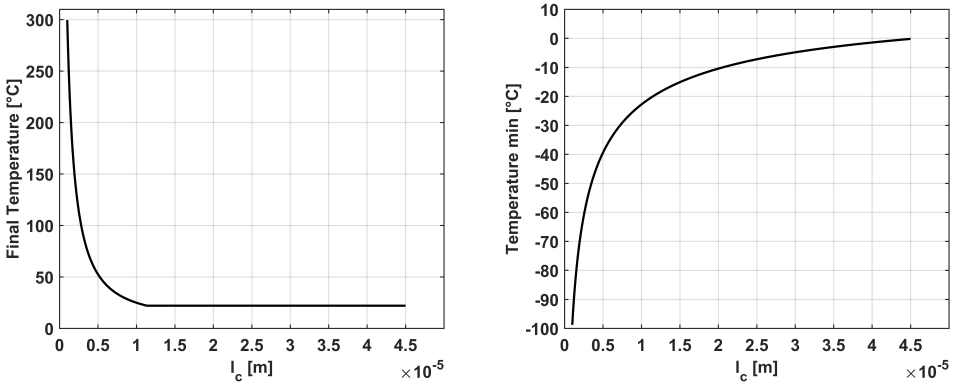

FIGURE 8: Final value of the temperature (at $d = 1$) and its minimal value (at the end of the cooling phase) versus the size of the microstructure l_c.

remains available for damage.

The process is accompanied by a temperature drop in the elastic regime followed by a reverse tendency during damage growth. For small l_c, the damage propagates rapidly with more dissipated energy converted to heat. This leads to a more rapid temperature rise up to quite elevated values. For large l_c, the damage rate is less important and so is the corresponding dissipation heating. Consequently, the temperature evolution is not so rapid and its final value is smaller.

Figure 8 shows the final values of the temperature, at complete failure, and its minimum values, corresponding to the end of the elastic cooling phase, for different sizes of the microstructure. For l_c of the order of a few microns, the temperature at failure may be of hundreds of degrees while for l_c of some tens of microns we reach an asymptotic value of about ten degrees Celsius. For small values of l_c the evolution of $T^{(0)}$ passes through low negative values,

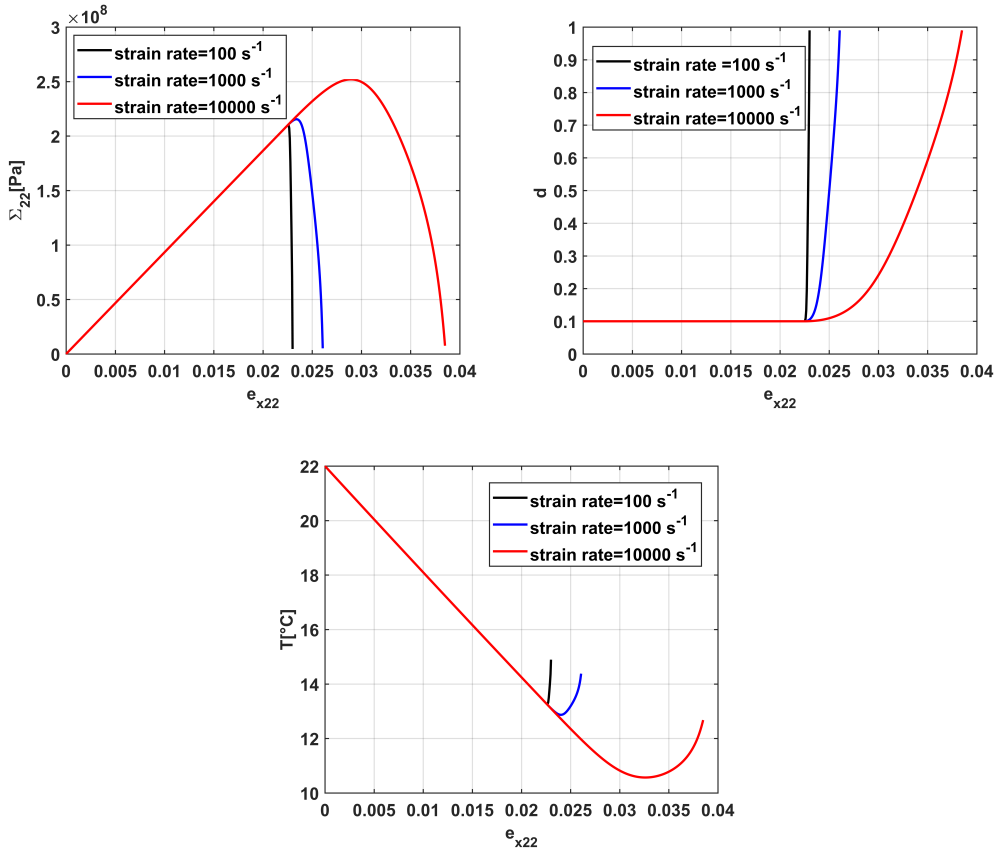

FIGURE 9: Effective stress, damage and temperature for different strain rates : $\dot{e}_{x22} = 100\ s^{-1}$, $\dot{e}_{x22} = 1000\ s^{-1}$ and $\dot{e}_{x22} = 10000\ s^{-1}$.

while for higher microstructural lengths the minimum temperature is of about $0\,°C$.

Globally, the damage behavior for finer microstructures is more brittle with higher dynamic tensile strength and this induces more substantial temperature variations during both cooling and heating regimes.

5.2.3. Influence of the rate of loading

We study now the influence of the loading rate. The effective stress, damage and temperature are represented in Fig. 9 for three strain rates : $\dot{e}_{x22} = 100\ s^{-1}$, $\dot{e}_{x22} = 1000\ s^{-1}$, $\dot{e}_{x22} = 10000\ s^{-1}$. The microscopic length parameter is chosen $l_c = 3 \times 10^{-4}\, m$.

As already observed in the purely mechanical case (Keita et al., 2014), the increase of the loading rate induces more ductility in the macroscopic response of the material. This is the consequence of the inertial effects incorporated in the damage model. At high strain rates, a more important part of the supplied energy is stored as kinetic energy around microcrack tips, causing a slowing effect in the propagation of microcracks. Consequently, the dynamic strength is increased and the response in the evolving damage regime is more ductile, as can be observed in the plotted stress and damage evolutions.

When the damage initiation is retarded, the cooling regime is extended as show the temperature curves in Fig. 9. Since the damage rate controls the amount of energy converted to heat, for higher loading rates the model predicts lower heat production during the propagation phase. Finally, the temperature curves in Fig. 9 are the consequence of the competition between the duration of the heating regime and the amount of energy dissipated as heat. For high strain rates, the dissipation is less important but the heating time is longer, while for slower strain evolutions more substantial amounts of energy are dissipated in shorter times, due to the rapid damage growth.

It worths remarking that for smaller microstructural sizes the ductility is substantially reduced and the heating increases considerably leading to

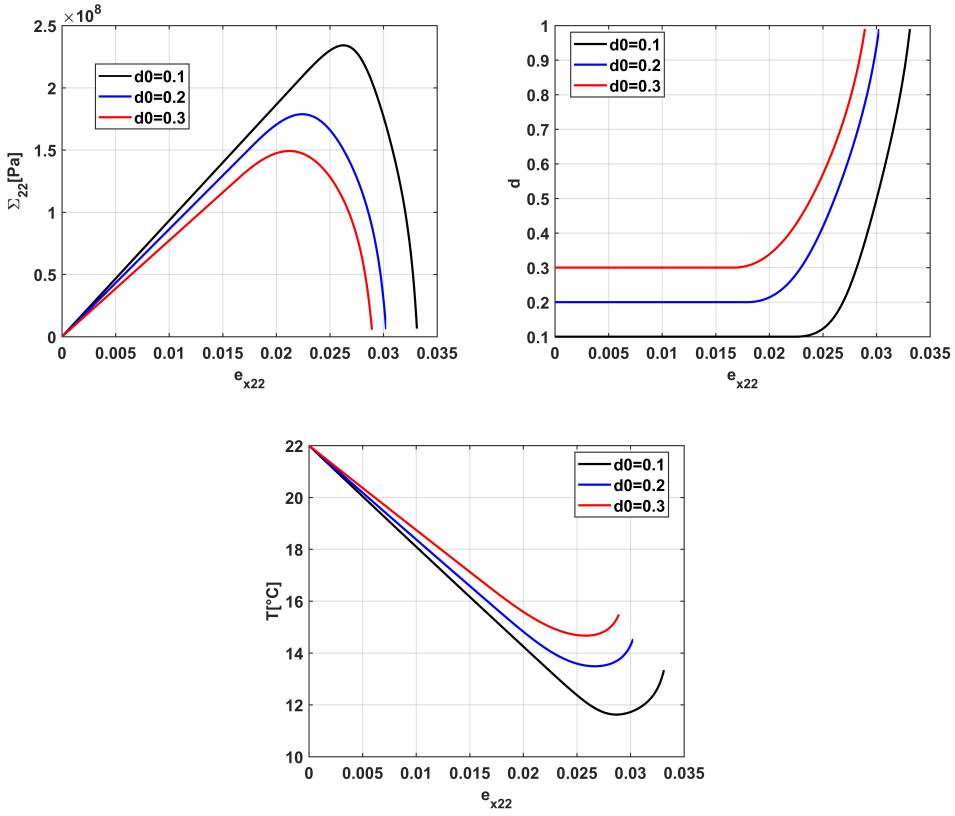

FIGURE 10: Macroscopic fields for initial values of damage : $d_0 = 0.1$, $d_0 = 0.2$ and $d_0 = 0.3$.

elevated final temperatures for a larger range of strain rates. This effect can be observed by comparison with the temperature curves in Figures 6 and 7.

5.2.4. Influence of the initial damage

We finally study the role of the initial value of damage d_0. The response of the model is represented in Fig. 10 for $d_0 = 0.1$, $d_0 = 0.2$ and $d_0 = 0.3$ and the small-scale length $l_c = 3 \times 10^{-4}\, m$.

As expected, smaller values of d_0 lead to higher tensile strengths, retar-

ded damage initiation but followed by a more rapid evolution. The stiffness decreases with the increase of the initial damage.

The retarded damage initiation increases the elastic cooling regime such that the minimum temperature is lower for smaller d_0. During the propagation phase, the faster evolution of damage obtained for smaller d_0 leads to increased heating such that the temperature rise is more important. For higher values of d_0, the heating phase starts earlier and the final temperature is higher even if the damage rate and the associated heating are smaller.

6. Numerical Simulation of the Compact Compression Test

We present in this section numerical simulations of the Compact Compression Test (CCT) and we compare the results with the experimental data reported in Rittel (1998, 1999); Bougaut and Rittel (2001) for thermal evolutions during failure initiation and propagation phases.

The geometry of the CCT specimen is shown in Figure 11. The material is the commercial polymethylmethacrylate (PMMA). An impact loading is applied through a Hopkinson steel bar of $16.5\,mm$ diameter such that tensile failure is initiated in the upper part, at the tip of a pre-existing notch where a small fatigue crack has been processed. Impact velocities in the range $8 - 65\,m/s$ have been applied. The specimen is instrumented with a fracture gage and an embedded thermocouple, allowing measurements of the fracture time and the temperature in the vicinity of the tip. The fracture gage and the thermocouple are placed at $1\,mm$ distance ahead of the fatigue crack tip.

Under impact loading, mixed mode fracture is initiated at the tip of the pre-existing crack and traverses the specimen vertically following a slightly

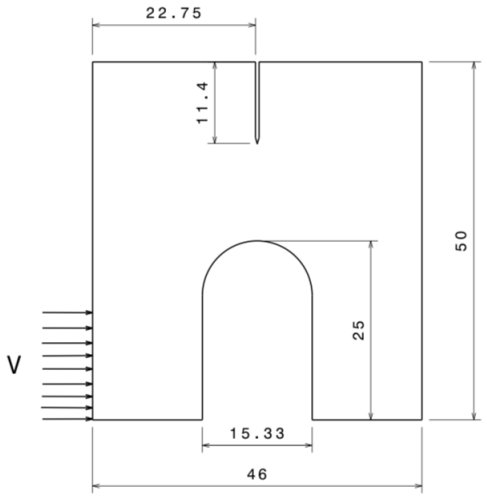

FIGURE 11: Geometry of the CCT specimen, with dimensions in mm. The impact velocity V is applied over a region of $16.5\,mm$.

curved path in dominant mode I propagation. The measurements show that, prior to failure initiation, the near-tip temperature can drop by several tens of degrees. This cooling phase is followed by a significant temperature rise during the fracture growth, the crack tip behaving like a heat source. In this heating phase, the temperatures at the tip can mount up to a few tens of degrees higher than the initial temperature of the specimen. Such thermal variations indicate the necessity of adopting a thermo-mechanical framework for the modeling of dynamic failure.

As shown for instance in Bougaut and Rittel (2001) and Bjerke and Lambros (2003), adiabatic conditions can be reasonably assumed in the description of such dynamic fracture tests and for short time intervals around the failure initiation instant. In the present simulations we assume macroscopic adiabatic conditions by neglecting the conduction term in the left-hand side

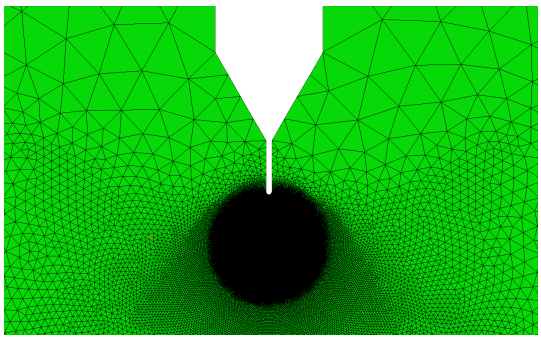

FIGURE 12: Local geometry near the notch tip and finite element mesh with refinement in the failure initiation zone.

of the temperature equation (80).

To simulate the compact compression experiment, we implemented the thermoelastic damage model as a ABAQUS VUMAT user material subroutine using explicit time integration. Under the adiabaticity condition, dynamic elasticity computations can be performed in Abaqus Explicit with the complete resolution of the temperature and damage equations in the user subroutine. On a time step and for given strain increments in an integration point of the FE mesh, we first solve the damage law (79) using a Euler forward scheme, with the temperature value at the beginning of the step and a non-decreasing numerical condition for damage. Then, with the computed damage at the end of the time step, a forward Euler scheme is also employed for the adiabatic temperature equation (80). After the computation of the new values of temperature and damage, the stress components are updated according to the constitutive relation (5).

A FE mesh is constructed with plane strain 3-nodes linear elements CPE3. The local geometry near the notch tip and the finite element mesh refined

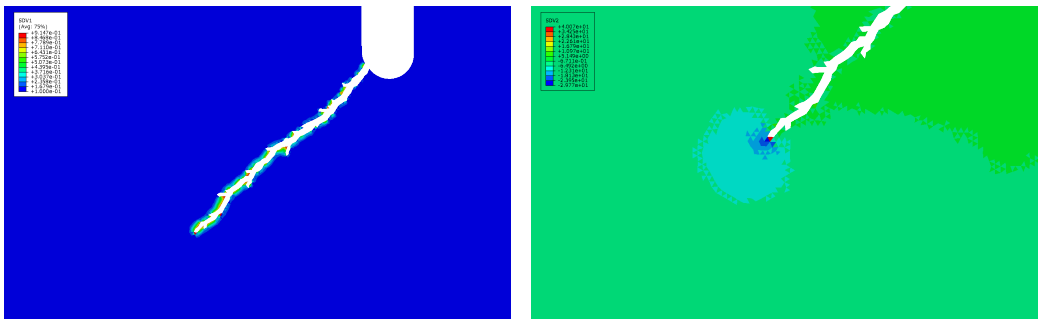

FIGURE 13: Left : damage variable represented with element deletion at complete failure. Right : temperature field with cooling and heating zones near the moving tip.

in the region of expected rupture initiation are shown in Figure 12. The length of the "fatigue crack" is $0.5\,mm$ and its thickness is $0.05\,mm$ with a rounded tip (magnified in Fig. 13). The element size in the region near the tip is about $0.003\,mm$. The impact loading is modeled by an applied velocity $V = 30\,m/s$ over a boundary zone of $16.5\,mm$, as in Fig. 11, corresponding to the diameter of the Hopkinson bar.

The material parameters of the PMMA material are those given in the beginning of Section 5 and the microstructural length value is chosen as $l_c = 6\times10^{-5}\,m$. Since the relevant macroscopic dimensions L_c of the specimen are of order of tens of milimeters, the separation of scales assumption (14) is verified.

In the left side of Figure 13, the computed damage variable d is represented. Element deletion is activated at the damage value $d = 0.99$. We note the initiation of a macrocrack with a kink angle with respect to the vertical direction ; such a failure path deviation can be retrieved in the experimental observations (Rittel, 1998). Microbranching effects are observed in the

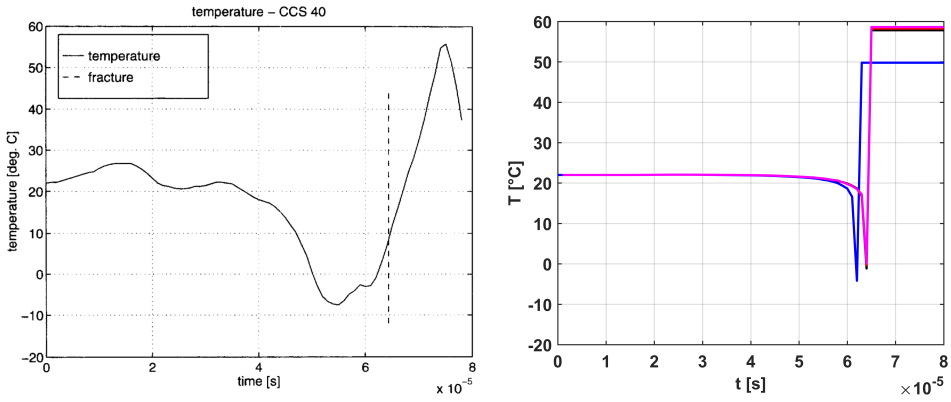

FIGURE 14: Temperature variation at $1\,mm$ from the tip of the notch : measured values (left) from Rittel (1998) and computed values (right) in 4 neighbor elements in the area of the thermocouple location.

damaged zone.

The computed temperature field near the tip of the propagating macro-crack is shown in the right image of Figure 13. Ahead of the tip a cooling zone is present, with a minimum relative temperature of about $-30°C$, while the tip is behaving like a heat source with a maximum relative temperature of about $40°C$. In Figure 13, the temperature is represented without average element output at nodes. The obtained temperature distribution is the consequence of the small-scale heating accounted by the damage model.

We note that the highly localized heat source in Fig. 13 is in agreement with experimental results of Fuller et al. (1975) who estimated the width of the hot zone along the crack path to be about $1-3\,\mu m$, which also corresponds to the observed maximal craze thickness in PMMA (e.g., Döll, 1983).

The measured values of the temperature at $1\,mm$ from the tip of the notch reported in Rittel (1998) are given in Figure 14 together with the correspon-

ding computed values in four elements situated in the same region. Similar temperature variations can be noticed : a cooling regime with a temperature drop of about $25 - 30°C$ from the initial value $T_0 = 22°C$, followed by a heating regime in which the rise of the temperature may be of $30 - 35°C$.

These results confirm the capacity of the model to correctly predict the thermal evolutions associated with the dynamic failure of brittle materials.

7. Conclusions

We constructed a coupled thermo-mechanical damage model for brittle materials based on dynamic evolutions of microcracks with dissipated fracture energy converted to heat at propagating tips.

Starting with a distribution of microcracks propagating according to a Griffith type criterion in dynamics and with point heat sources at the moving tips, a homogenization method based on asymptotic developments has been employed to deduce a damage evolution law coupled with the thermoelasticity system at the macroscale. The upscaling procedure leads to distributed heat sources, related to the damage energy-release rate, in the homogenized temperature equation and the damage law depend on the thermal and the mechanical fields, such that the obtained macroscopic system has strong thermo-mechanical-damage couplings.

While the failure heating effect has been addressed previously in the framework of Fracture Mechanics, through models of crack-tip heat sources (e.g., Bui et al., 1980, 1986; Sun and Hsu, 1996) or thermally dissipative cohesive zones (Bjerke and Lambros, 2003; Estevez et al., 2005), the present approach appears to be the first one proposing a multiscale description of the heating

due to distributed damage evolution in dynamics.

The local effective response of the model has been analyzed with special emphasis on thermal evolutions. Strain-rate and size effects related to the length of the microstructure are illustrated for strain-driven evolutions of stress, damage and temperature. Cooling effects prior to damage initiation and heating during propagation have been illustrated for different model parameters.

Numerical simulations have been performed to reproduce the compact compression test for PMMA samples. Comparisons with the temperature field measurements during rapid failure reported in Rittel (1998) have shown good agreement between theoretical predictions and experimental results.

Acknowledgments The research leading to these results has received funding from the European Union's Horizon 2020 Programme (Excellent Science, Marie-Sklodowska-Curie Actions) under REA grant agreement 675602 (Project OUTCOME).

Appendix

By retaining the first two terms in the asymptotic developments (15-16) of displacements and temperature, we obtain the expression of the energy-release rate

$$\mathcal{G}^{d\varepsilon} = \frac{1}{\varepsilon}\mathcal{G}^{(-1)} + \mathcal{G}^{(0)} + \varepsilon\mathcal{G}^{(1)} + \varepsilon^2\mathcal{G}^{(2)} + \varepsilon^3\mathcal{G}^{(3)} \tag{81}$$

where the terms of different orders are :

$$\mathcal{G}^{(-1)} = \lim_{r\to 0}\int_{\Gamma Y_r} (\frac{1}{2}(\lambda e_{yii}(\mathbf{u}^{(0)})e_{yjj}(\mathbf{u}^{(0)}) + 2\mu e_{yij}(\mathbf{u}^{(0)})e_{yij}(\mathbf{u}^{(0)}))n_1 \\ -(\lambda e_{ykk}(\mathbf{u}^{(0)})\delta_{ij} + 2\mu e_{yij}(\mathbf{u}^{(0)}))n_j \frac{\partial u_i^{(0)}}{\partial y_1})\ ds_y \qquad (82)$$

$$\mathcal{G}^{(0)} = \lim_{r\to 0}\int_{\Gamma Y_r} (\lambda e_{yii}(\mathbf{u}^{(0)})(e_{xjj}(\mathbf{u}^{(0)}) + e_{yjj}(\mathbf{u}^{(1)})) \\ +2\mu e_{yij}(\mathbf{u}^{(0)})(e_{xij}(\mathbf{u}^{(0)}) + e_{yij}(\mathbf{u}^{(1)})) + (3\lambda+2\mu)\alpha T_0 e_{ykk}(\mathbf{u}^{(0)}))n_1 \\ -(\lambda(e_{xkk}(\mathbf{u}^{(0)}) + e_{ykk}(\mathbf{u}^{(1)}))\delta_{ij} + 2\mu(e_{xij}(\mathbf{u}^{(0)}) + e_{yij}(\mathbf{u}^{(1)})))n_j \frac{\partial u_i^{(0)}}{\partial y_1} \\ -(\lambda e_{ykk}(\mathbf{u}^{(0)})\delta_{ij} + 2\mu e_{yij}(\mathbf{u}^{(0)}))n_j(\frac{\partial u_i^{(0)}}{\partial x_1} + \frac{\partial u_i^{(1)}}{\partial y_1}))\ ds_y \qquad (83)$$

$$\mathcal{G}^{(1)} = \lim_{r\to 0}\int_{\Gamma Y_r} (\frac{1}{2}(\lambda(2e_{yii}(\mathbf{u}^{(0)})e_{xjj}(\mathbf{u}^{(1)}) + (e_{xii}(\mathbf{u}^{(0)}) + e_{yii}(\mathbf{u}^{(1)}))^2) \\ +2\mu(2e_{yij}(\mathbf{u}^{(0)})e_{xij}(\mathbf{u}^{(1)}) + (e_{xij}(\mathbf{u}^{(0)}) + e_{yij}(\mathbf{u}^{(1)}))(e_{xij}(\mathbf{u}^{(0)}) + e_{yij}(\mathbf{u}^{(1)})) \\ +(3\lambda+2\mu)\alpha T_0(e_{xkk}(\mathbf{u}^{(0)}) + e_{ykk}(\mathbf{u}^{(1)})) + cT^{(0)} + \frac{\rho}{8}\frac{\partial u_i^{(0)}}{\partial y_1}\frac{\partial u_i^{(0)}}{\partial y_1}(\frac{dd}{dt})^2)n_1 \\ -(\lambda e_{ykk}(\mathbf{u}^{(0)})\delta_{ij} + 2\mu e_{yij}(\mathbf{u}^{(0)})n_j(\frac{\partial u_i^{(1)}}{\partial x_1} + \frac{\partial u_i^{(2)}}{\partial y_1}) \\ -(\lambda(e_{xkk}(\mathbf{u}^{(0)}) + e_{ykk}(\mathbf{u}^{(1)}))\delta_{ij} + 2\mu(e_{xij}(\mathbf{u}^{(0)}) + e_{yij}(\mathbf{u}^{(1)})))n_j(\frac{\partial u_i^{(0)}}{\partial x_1} + \frac{\partial u_i^{(1)}}{\partial y_1}) \\ -(\lambda e_{xkk}(\mathbf{u}^{(1)})\delta_{ij} + 2\mu e_{xij}(\mathbf{u}^{(1)}))n_j\frac{\partial u_i^{(0)}}{\partial y_1})\ ds_y \qquad (84)$$

$$\mathcal{G}^{(2)} = \lim_{r\to 0}\int_{\Gamma Y_r} (cT^{(1)})n_1\ ds_y + {L_c}^2 \lim_{r\to 0}\int_{\Gamma Y_r} (\frac{\rho}{4}\frac{\partial u_i^{(0)}}{\partial y_1}(\frac{\partial u_i^{(0)}}{\partial x_1} + \frac{\partial u_i^{(1)}}{\partial y_1})(\frac{dd}{dt})^2)n_1\ ds_y \qquad (85)$$

$$\mathcal{G}^{(3)} = {L_c}^2 \lim_{r\to 0}\int_{\Gamma Y_r} \frac{\rho}{8}(\frac{dd}{dt})^2(2\frac{\partial u_i^{(0)}}{\partial y_1}\frac{\partial u_i^{(1)}}{\partial x_1} + (\frac{\partial u_i^{(0)}}{\partial x_1} + \frac{\partial u_i^{(1)}}{\partial y_1})(\frac{\partial u_i^{(0)}}{\partial x_1} + \frac{\partial u_i^{(1)}}{\partial y_1}))\ ds_y \qquad (86)$$

For the velocity field the local relation $\frac{\partial u_i^\varepsilon}{\partial t} \simeq -\frac{d(l/2)}{dt}\frac{\partial u_i^\varepsilon}{\partial x_1} = -\frac{\varepsilon L_c}{2}\frac{dd}{dt}\frac{\partial u_i^\varepsilon}{\partial x_1}$ in the vicinity of the crack tips (Freund, 1990; Bui et al., 1980) has been used.

Since $\mathbf{u}^{(0)}$ and $T^{(0)}$ are independent of the y variable, some of the terms in the above expressions are vanishing. And if we take into account the singularity of $\mathbf{u}^{(1)}(\mathbf{y})$ and $T^{(1)}(\mathbf{y})$ at the crack tips, we deduce that $\mathcal{G}^{(-1)} = \mathcal{G}^{(0)} = \mathcal{G}^{(2)} = 0$.

Finally, the only non-vanishing terms in the development of $\mathcal{G}^{d\varepsilon}$ are :

$$\mathcal{G}^{d\varepsilon} = \varepsilon \mathcal{G}^{(1)} + \varepsilon^3 \mathcal{G}^{(3)} \tag{87}$$

where :

$$\mathcal{G}^{(1)} = \lim_{r\to 0} \int_{\Gamma Y_r} (\frac{1}{2}(\lambda e_{yii}(\mathbf{u}^{(1)}) e_{yjj}(\mathbf{u}^{(1)}) + 2\mu e_{yij}(\mathbf{u}^{(1)}) e_{yij}(\mathbf{u}^{(1)})))n_1 \\ -(\lambda e_{ykk}(\mathbf{u}^{(1)}))\delta_{ij} + 2\mu e_{yij}(\mathbf{u}^{(1)}))n_j \frac{\partial u_i^{(1)}}{\partial y_1}) ds_y \tag{88}$$

$$\mathcal{G}^{(3)} = {L_c}^2 \lim_{r\to 0} \int_{\Gamma Y_r} \frac{\rho}{8} (\frac{dd}{dt})^2 \frac{\partial u_i^{(1)}}{\partial y_1} \frac{\partial u_i^{(1)}}{\partial y_1} \, ds_y \tag{89}$$

The kinetic energy only contributes to the term $\mathcal{G}^{(3)}$ of the above development of the dynamic energy release rate. The term of order ε can be obtained in (87) by considering higher order correctors for the thermomechanical fields.

References

Allix, O., Feissel, P., Thévenet, P., 2003. A delay damage mesomodel of laminates under dynamic loading : basic aspects and identification issues. Comput. Struct., 81, 1177-1191.

Auriault, J.-L., 2012. Wave propagation and transient heat transfer in thermoelastic composites. Int. J. Heat Mass Transfer 55, 5972-5978.

Berry, J.P., 1960. Surface characteristics of fractured poly(methyl methacrylate). Nature 185 (4706), 91-92.

Bhatt, H., Rosakis, A., Sammis, G., 2011. A micro-mechanics based constitutive model for brittle failure at high strain rates. J. Appl. Mech. 79, 1016-1028.

Bjerke, T. W., Lambros, J., 2003. Theoretical development and experimental validation of a thermally dissipative cohesive zone model for dynamic fracture of amorphous polymers, J. Mech. Phys. Solids 51, 1947-1970.

Borden, M.J., Verhoosel, C.V., Scott, M.A., Hughes, T.J.R., Landis, C.M., 2012. A phase-field description of dynamic brittle fracture. Comp. Meth. Appl. Mech. Engng. 217-220, 77-95.

Bourdin, B., Larsen, C.J., Richardson, C., 2011. A time-discrete model for dynamic fracture based on crack regularization. Int. J. Fract. 168, 133-143.

Bougaut, O., Rittel, D., 2001. On crack-tip cooling during dynamic crack initiation, Int. J. Solids Struct. 38, 2517-2532.

Bui, H.D., Ehrlacher, A., Nguyen, Q.S., 1980. Propagation de fissure en thermoélasticité dynamique, J. Mécanique, 19, 697-723.

Bui, H.D., Ehrlacher, A., Nguyen, Q.S., 1986. Thermomechanical couplings in fracture mechanics. In *Thermomechanical couplings in solids*, eds. H.D. Bui and Q.S. Nguyen, Elsevier Amsterdam, North Holland, 327-341.

Chu, D., Li, X., Liu, Z., 2017. Study the dynamic crack path in brittle material under thermal shock loading by phase field modeling. Int. J. Fract. 208, 114-130.

Dalmas, D., Guerra, C., Scheibert, J., Bonamy, D., 2013. Damage mechanisms in dynamic fracture of nominally brittle polymers, Int. J. Fract. 184, 93-111.

Dascalu, C., Bilbie, G., Agiasofitou, E., 2008. Damage and size effect in elastic solids : a homogenization approach. Int. J. Solids Struct. 45, 409-430.

Dascalu, C., François, B., Keita, O., 2010. A two-scale model for subcritical damage propagation. Int. J. Solids Struct., 47, 493-502.

Dascalu, C., 2017. Dynamic localization of damage and microstructural length influence. Int. J. Damage Mech. 28, 1190-1218.

Dascalu, C., 2018. Multiscale modeling of rapid failure in brittle solids : branching instabilities. Mech. Mater., 116, 77-89.

Döll, W., 1983. Optical interference measurements and fracture mechanics analysis of crack tip craze zones. Adv. Polymer Science 52-53, 105-168.

Dubé, J.F., Pijaudier-Cabot, G., La Borderie, C., 1996, Rate dependent damage model for concrete in dynamics, J. Engng. Mech. 122, 939-947.

Ene, H.I., 1983. On linear thermoelasticity of composite materials, Int. J. Engng. Sci. 21, 443-448.

Estevez, R., Basu, S., van der Giessen, E., 2005. Analysis of temperature effects near mode I cracks in glassy polymers. Int J. Fract. 132, 249-273.

Fish, J., 2013. Practical Multiscaling. John Wiley & Sons.

François, B., Dascalu, C., 2010. A two-scale time-dependent damage model based on non-planar growth of micro-cracks, J. Mech. Phys. Solids 58, 1928-1946.

Francfort, G.A., 1983. Homogenization and linear thermoelasticity, SIAM J. Math. Anal. 14, 696-708.

Freund, L.B., 1990. Dynamic Fracture Mechanics. Cambridge University Press.

Fuller, K.N.G., Fox, P.G., Field, J.E., 1975. The temperature rise at the tip of a fast-moving crack in glassy polymers. Proc. R. Soc. London A341, 537-557.

Hofacker, M., Miehe, C., 2012. Continuum phase field modeling of dynamic fracture : variational principles and staggered FE implementation. Int. J. Fract. 178, 113-129.

Hu, G., Liu, J., Graham-Brady, L., Ramesh, K.T., 2015. A 3D mechanistic model for brittle materials containing evolving flaw distributions under dynamic multiaxial loading. J. Mech. Phys. Solids 78, 269-297.

Huang, C., Subhash, G., Vitton, S.J., 2002. A dynamic damage growth model for uniaxial compressive response of rock aggregates. Mech. Mater. 34, 267-277.

Kalpakides, V.K., Dascalu, C., 2002. On the Thermomechanical Formulation of Configurational Forces in Continua, Proc. R. Soc. London, A 458, 1-17.

Keita, O., Dascalu, C., François B., 2014. A two-scale model for dynamic damage evolution. J. Mech. Phys. Solids. 64, 170-183.

Li, T., Marigo, JJ., Guilbaud, D., Potapov, S., 2016. Gradient damage modeling of brittle fracture in an explicit dynamics context. Int. J. Num. Meth. Engng. 108, 1381-1405.

Markenscoff, X., Dascalu, C., 2012. Asymptotic homogenization analysis for damage amplification due to singular interaction of microcracks. J. Mech. Phys. Solids 60, 1478-1485.

Miehe, C., Schanzel, L.M., Ulmer Heike., 2015. Phase field modeling of fracture in multi-physics problems. Part I. Balance of crack surface and failure criteria for brittle crack propagation in thermo-elastic solids. Comp. Meth. Appl. Mech. Engng. 294, 449-485.

Nemat-Nasser, S., Deng, H., 1994. Strain-rate effect on brittle failure in compression. Acta Metall. Mater. 42, 1013-1024.

Parnell, W.J., 2006. Coupled thermoelasticity in a composite half-space, J. Eng. Math. 56, 1-21.

Paliwal, B., and Ramesh, K. T., 2008. An Interacting Micro-Crack Damage Model for Failure of Brittle Materials Under Compression, J. Mech. Phys. Solids, 56, 896-923.

Ravi-Chandar, K., Knauss, WG., 1984. An experimental investigation into dynamic fracture : II. Microstructural aspects. Int J. Fract. 26, 65-80.

Ravi-Chandar, K., Yang, B., 1997. On the role of microcracks in the dynamic fracture of brittle materials, J. Mech. Phys. Solids 45, 535-563.

Ravi-Chandar, K., 2004. Dynamic fracture. Boston. Elsevier.

Ravichandran, G., Subhash, G., 1995. A micromechanical model for high strain rate behavior of ceramics. Int. J. Solids Struct. 32, 2627-2646.

Rittel, D., 1998. Experimental investigation of transient thermoelastic effects in dynamic fracture, Int. J. Solids Struct. 35, 2959-2973.

Rittel, D., 1999. Thermomechanical aspects of dynamic crack initiation, Int. J. Fract. 99, 199-209.

Sanchez-Palencia, E., 1980. Non-homogeneous Media and Vibration Theory. Lecture Notes in Physics, vol.127, Springer, Berlin.

Schlüter, A., Willenbücher, A., Kuhn, C., Müller, R., 2014. Phase field approximation of dynamic brittle fracture. Comp. Mech. 54, 1141-1161.

Schlüter, A., Kuhn, C., Müller, R. Tomut, M., Trautmann, C., Weick, H., Plate, C., 2017. Phase field modelling of dynamic thermal fracture in the context of irradiation damage. Continuum Mech. Thermodyn. 29, 977-988.

Sharon, E., Gross, SP., Fineberg, J., 1996. Energy dissipation in dynamic fracture. Phys. Rev. Lett. 76, 2117-2120.

Sharon, E., Fineberg, J., 1999. Confirming the continuum theory of dynamic brittle fracture for fast cracks. Lett. Nature 397, 333-335.

Spatschek, R., Brener, E., Karma, A., 2011. Phase field modeling of crack propagation, Phil. Mag., 91, 75-95.

Suffis, A., Lubrecht, T.A.A., Combescure A., 2003. Damage model with delay effect. Analytical and numerical studies of the evolution of the characteristic damage length. Int. J. Solids Struct. 40, 3463-3476.

Sun, N.S., Hsu, T.R., 1996. Thermomechanical coupling effects on fractured solids. Int. J. Fract. 78, 67-87.

Weichert, R., Schönert, K., 1978. Heat generation at the tip of a moving crack. J. Mech. Phys. Solids 26, 151-161.

Wool, R.P., 1995. Polymer Interfaces : Structure and Strength. Hanser Publishers, New York.